Applied Thermal Engineering 297 (2026) 130827

Contents lists available at ScienceDirect

Applied Thermal Engineering

journal homepage: www.elsevier.com/locate/apthermeng

Research Paper

Enhancing annual performance in air/ground dual-source heat pumps coupled to undersized borehole heat exchangers through variable source-selection logics

Claudia Naldi, Christian Natale, Matteo Dongellini *, Gian Luca Morini

Department of Industrial Engineering, Alma Mater Studiorum – University of Bologna, Viale del Risorgimento 2, 40136, Bologna, Italy

ARTICLE INFO

Keywords:
Dual-source heat pump
Air-source heat pump
Geothermal heat pump
Source-selection logic
Borehole heat exchanger
Numerical analysis

ABSTRACT

The energy performance of conventional Air-Source Heat Pumps (ASHPs) decreases significantly as the external air temperature drops, whereas Ground-Coupled Heat Pumps (GCHPs) are characterized by high borefield investment costs and risk of performance decline over time due to unbalanced building loads. To address these issues, this paper investigates the seasonal ($SCOP_{net}$) and annual (APF_{net}) energy performance of a Dual-Source Heat Pump (DSHP) able to exploit alternately aerothermal and geothermal energy, comparing it with that of conventional ASHPs and GCHPs through long-term simulations. A building with strongly unbalanced loads is considered, coupled to borefields up to 50% undersized. Three source-selection logics are examined: (i) setting of a switching temperature based on ambient air (ST logic); (ii) source selection as a function of time (SP logic); (iii) source determination based on DSHP instantaneous *COP* for both operating modes (PCOP logic). The ASHP exhibits the lowest performance (APF_{net} equal to 2.67), whereas the DSHP and GCHP yield 10–37% improvements. The source-selection strategy and borefield size play a key role in the DSHP performance: the SP logic offers minimal benefits, while ST and PCOP strategies guarantee up to +9% in $SCOP_{net}$, +8% in APF_{net} and −7% in electric energy consumption compared to conventional GCHPs. The shorter the borefield, the higher the advantage of using a DSHP with ST or PCOP control logic. The findings highlight the potential of DSHPs in applications with strongly unbalanced loads, or in retrofitting heat generators in existing geothermal-based HVAC systems when the borefield becomes undersized over time.

1. Introduction

The dramatic increase in greenhouse gas emissions over the last decades has led to global warming and climate change [1]. Since the largest share of emissions is linked to fossil fuel combustion for anthropogenic activities [2], there is an urgent need to boost the deployment of renewable energy sources. Within this framework, the building sector contributes a significant share of the emissions released. In advanced economies, such as those in the European Union, buildings account for up to 16% of emissions [3], primarily due to space heating and hot water demands [4]. In this regard, a rapid transition from traditional heating systems to low-emission technologies driven by electricity must be accelerated to reduce the building sector footprint. Vapor-compression heat pumps are suitable candidates for replacing fossil fuel-based heat generators, as they provide heating, cooling, and domestic hot water with high efficiency, thereby reducing electric energy consumption [5]. Currently, several energy sources can be deployed as heat sources or sinks by this kind of system based on building features (e.g., available outdoor space, energy demand) and climatic factors. Typical heat sources/sinks include air, ground, waste heat, and water [6]. It is also worth mentioning that external sources have a significant impact on the heat pump performance, affecting its heating/cooling capacity, overall efficiency, and the working temperature range [7]. Since water-source and waste heat-source heat pumps are not widely adopted due to a scarce availability of these sources and regulatory restrictions, air-source heat pumps (ASHPs) and ground-coupled heat pumps (GCHPs) are the most widely adopted technologies in residential and non-residential buildings [8]. Their main features can be summarized as follows:

(i) Due to the extremely high availability of the ambient air as external heat source/sink, ASHPs are the most widespread solution on the market. In the European Union, almost 98% of units

* Corresponding author.
E-mail address: matteo.dongellini@unibo.it (M. Dongellini).

https://doi.org/10.1016/j.applthermaleng.2026.130827
Received 13 January 2026; Received in revised form 12 March 2026; Accepted 28 March 2026
Available online 30 March 2026

Nomenclature

APF	Annual Performance Factor
COP	Coefficient of Performance
c_p	Specific heat capacity at constant pressure [J kg^{-1} K^{-1}]
D	Diameter [m]
EER	Energy Efficiency Ratio
k	Thermal conductivity [W m^{-1} K^{-1}]
L	Length [m]
Q	Thermal energy [kWh]
RH	Relative Humidity [%]
s	Shank spacing [m]
SCOP	Seasonal Coefficient of Performance
SEER	Seasonal Energy Efficiency Ratio
T	Temperature [°C]
W	Electric energy [kWh]

Greek symbols

α	Thermal diffusivity [m^2 s^{-1}]
β	Heat pump electric power input reduction factor
γ	Heat pump heating capacity reduction factor
Δ	Difference
ν	Kinematic viscosity [m^2 s^{-1}]
ρ	Density [kg m^{-3}]
τ	Time [s]

Subscripts

a	indoor air
b	borehole
c	cooling
e	external
el	electric
f	fluid
gnd	ground
gt	grout
h	heating
i	internal
ice	freezing
in	inlet
net	net
nom	nominal
out	outlet
p	pipe
th	thermal
und	undisturbed
w	water

Acronyms

ASHP	Air-Source Heat Pump
BHE	Borehole Heat Exchanger
DSHP	Dual-Source Heat Pump
GCHP	Ground-Coupled Heat Pump
HP	Heat Pump
HVAC	Heating, Ventilation and Air Conditioning
KPI	Key Performance Indicator
PCOP	Predicted Coefficient of Performance
RCD	Reverse Cycle Defrosting
SP	Sun Position
ST	Switching Temperature [°C]
TRY	Test Reference Year

sold in 2024 for heating and cooling purposes were constituted by aerothermal heat pumps [9]. However, their energy performance depends strongly on ambient air conditions, and a significant penalty to heating capacity and efficiency is incurred with low values of the external air temperature, particularly in correspondence with the frosting phenomenon on the evaporator surface [10].

(ii) GCHPs present higher efficiency than ASHPs on a year-round basis thanks to the deployment of the ground as external heat source/sink, which presents a better thermal level and lower fluctuations than ambient air [11]. Nonetheless, unbalanced building thermal loads can lead to a significant drift in soil temperature over the years, and, consequently, a substantial decrease in heat pump performance [12]. Moreover, the installation of GCHP systems is accompanied by high capital investments due to the high drilling costs required for borefield installation [13].

In order to address the issues mentioned above, thermal source integration represents a suitable solution that has been studied by researchers and manufacturers [14]. In this sense, dual-source heat pumps (DSHPs) can exploit different thermal sources and deploy the most efficient one based on real-time operating conditions, such as air and ground temperatures, thereby enhancing the seasonal performance [15]. Moreover, these multi-source systems show specific benefits depending on the thermal source coupling. For example, air/ground DSHPs can relieve or avoid frosting during winter by switching to ground as the heat source when frost conditions occur [16]. Finally, although the complexity of heat pumps increases compared to single-source units, significant economies can be achieved in the overall installation costs of the HVAC system. Indeed, the availability of a second thermal source, namely air, allows for a reduction in the borefield size relative to a conventional GCHP of up to 50% [17], thereby decreasing the soil area requirement and the initial investment.

Within this framework, many papers have been published in recent years concerning the conceptualization, design, numerical simulation, and experimental verification of DSHP systems [18]. The air-source heat exchanger type, evaporator arrangement, and switch logic between thermal sources are the most influential and discussed parameters in this field. First, different coupling arrangements can be used for multiple heat sources on the evaporator side. Different heat exchangers can be arranged in parallel [19] or in series [20]. Alternatively, a specifically designed heat-exchange unit that allows simultaneous deployment of two thermal sources [21] can be adopted. With the former coupling method, solenoid valves are used to control refrigerant flow and select the operating heat exchanger, preventing interference between heat sources. Despite additional system complexity and pressure drops, the optimal thermal source can still be selected based on current operating conditions. On the contrary, arranging evaporators in series leads to a simpler configuration of the heat pump cycle, since no valves are needed. Still, higher pressure drops on the refrigerant flow are introduced, and a complex interference between the heat sources must be tackled. Integrating two or more thermal sources in a single heat exchanger is also an attempt to reduce the system complexity and volume. However, unifying multiple sources into a single component necessitates targeted design and higher processing costs, and dual-source operation requires the two thermal sources to be close in temperature. For these reasons, serial arrangement and integrated evaporators are not widely used in DSHP systems, and a parallel heat exchanger structure is typically adopted as the coupling method. Regarding the evaporator structure, the finned-tube coil is the most common heat exchanger typology on the air-source side of air/ground DSHPs, characterized by a relatively low heating capacity, as no additional outdoor equipment is

required [17]. A dry cooler or a cooling tower can replace the finned-tube heat exchanger for larger-capacity units. However, these solutions are not typically adopted due to the penalty on system efficiency and the increased complexity. On the DSHP ground-source side, plate heat exchangers are typically used [22]. Consequently, due to their small volume, the dimensions of DSHPs are close to those of conventional ASHPs, advantaging the system integration.

For all these reasons, the typical architecture of an air/ground heat pump consists of finned-tube and plate heat exchangers on the thermal source side, connected in parallel. In the open literature, several papers have been published demonstrating the advantages of this system. For instance, Corberan et al. [17] investigated the performance of an air/ground-to-water heat pump, manufactured as a plug-and-play unit, using a numerical model validated against experimental data obtained under steady-state conditions at a laboratory scale. They found that the DSHP could guarantee a comparable performance of a pure GCHP by halving the Borehole Heat Exchanger (BHE) area. More recently, Yu et al. [23] investigated the performance of a DSHP, arranged with two parallel evaporators and based on the utilization of air and waste heat as heat sources, using a validated numerical model. The dual-source unit could outperform a traditional ASHP by 70% at low ambient temperature values. An experimental study by Reum et al. [24] investigated the performance of a DSHP capable of utilizing both air and ground as heat sources, either alternately or simultaneously, through two compressors connected in parallel. Parallel operation yielded the major benefits, permitting the cover of the required heating load at reduced demand on the individual heat exchangers, and, therefore, allowing smaller dimensions of the heat exchange structures up to 58%. Several studies have shown that the effective year-round performance of DSHP systems is strongly influenced by the switching logic between thermal sources [25]. An improper control strategy could lead to long-term performance degradation, reduced efficiency and worsened indoor comfort conditions [26]. Therefore, optimizing the switch control and annual operation strategy of a DSHP is as significant as its design, and it is essential to maximize its performance. Most published studies considered a fixed value of the ambient air temperature as a threshold to switch between air-source and ground-source modes. Zarrella et al. [27] analyzed the retrofit of a GCHP system coupled to a cooling-dominant building that experienced a significant deterioration in the ground temperature. The inconvenience was solved with a dual-sink system that could reject heat to the ground or to the air. The switch logic was based on ambient air temperature: for values below 25 °C, the DSHP operated in air-source mode, whereas the ground loop was activated for values above 25 °C. The same logic was adopted by Zhang et al. [28]. They developed a mathematical model of a multi-source heat pump with five operating modes, aiming at evaluating the system energy, economic, and environmental performance. The control logic adopted for the DSHP mode was based on the outdoor air temperature: air was selected as the heat source when the ambient air temperature was above 5 °C; otherwise, the ground was used. Grossi et al. [29] proposed an improvement in the control algorithm of DSHP systems. Even though the switch between air-source and ground-source operation still relied on a fixed value of the ambient air temperature, the authors demonstrated that the DSHP performance could be maximized for a precise value of that parameter, depending on the size of the borefield coupled to the heat pump. In particular, the shorter the BHEs, the lower the optimal switching temperature. Similar results were obtained by Bordignon et al. [30]. A sensitivity analysis was carried out on the control parameters of an air/ground DSHP to minimize the long-term energy consumption. Heating and cooling loads, as well as the number of BHEs, varied across different scenarios, and the optimal value of the switching temperature was assessed. A different approach was followed by Zanetti et al. [31]. Numerical simulations performed on a DSHP operated in air-source and ground-source modes only allowed the development of a switching logic based on the difference between the ambient air temperature and the temperature of the water returning to the heat pump from the BHEs. When that difference was lower than 1.6 K, the DSHP operated in ground mode; otherwise, it operated in air mode. Although this control strategy enabled the selection of the heat source that provides the highest efficiency in real-time, it still relied on a fixed parameter determined in advance. Recently, some studies have proposed heat pump control strategies relying on machine learning approaches [32–34]. However, these works primarily aim to optimize the operation of single-source heat pumps or hybrid systems (heat pump and gas boiler) and, to date, have not yet been implemented in dual-source heat pump systems.

The energy, economic, and environmental benefits of DSHPs are clearly demonstrated by the papers published on this topic. However, the need for control optimization of these systems has increased accordingly to their diffusion. As noted in the literature analysis, the switch control is still based on simple algorithms, and further research is needed to improve the DSHP annual performance and boost the diffusion of this technology. Therefore, in this paper, three distinct control strategies are investigated to select the optimal thermal source for an air/ground DSHP, and their effectiveness is assessed through long-term numerical simulations in the Matlab-Simulink environment. In addition, different sizes of the BHE field coupled with the DSHP are simulated. The DSHP described in [29] is considered in this paper, and the influence of the heat source switch logic on the energy savings achievable with respect to conventional heat pumps is demonstrated. It is worth mentioning that the effective energy performance of the DSHP considered here was experimentally investigated in both air and ground modes [35]. Therefore, the outcomes of the present paper regarding the effectiveness of the different DSHP control algorithms are based on validated heat pump performance data. Consequently, this work aims to improve the energy performance of DSHPs by investigating the effects of different control logics and identifying borefield conditions where these systems can achieve greater energy-saving potential compared to traditional heat pumps, thereby boosting the diffusion of this technology. In addition, the presented outcomes can represent a benchmark for researchers and professionals aiming at optimizing the performance of DSHP systems.

2. Description of the case study

2.1. Building

The SFH100 archetype developed under IEA SHC Task 44 [36] was modeled as a reference building coupled to the DSHP to obtain reproducible and reliable results. This test house represents a non-renovated existing building, and the space heating energy demand is approximately 100 kWh m^{-2} y^{-1} under the European reference climate of Strasbourg. Since the authors are interested in investigating both the heating and cooling performance of the HVAC system and the effect of unbalanced building thermal loads, in this paper, the SFH100 building was located in Milan (Northern Italy), a site characterized by a cold winter and a humid summer. For the sake of convenience, the main thermo-physical characteristics of the building envelope components are reported in Table 1.

The heating season ranges from October 15th to April 15th (183 days) according to the current Italian regulation [37]. On the other hand, the cooling season is limited to 92 days, from June 1st to August 31st. The open-source Matlab-Simulink tool ALMABuild [38,39] was used to evaluate the building thermal loads by setting the indoor set-

Table 1
Main characteristics of the building envelope components.

	External walls	Floor	Roof	Windows
Thickness [cm]	26.8	36.5	9.5	2.0
Insulation thickness [cm]	1	4	4	–
Transmittance [W m^{-2} K^{-1}]	1.26	0.21	0.58	3.00

point temperature to 20 °C and 26 °C during winter and summer, respectively. The building thermal energy need for domestic hot water production is not considered in the present study. The Test Reference Year (TRY) for Milan from the CTI database [40] was used to obtain the hourly climatic data for the location. The heating and cooling design external air temperature values are −2 °C and 34 °C, respectively.

The results of the building numerical simulations indicate that the peak loads for space heating and space cooling are 7.4 kW and 3 kW, respectively. Consequently, the heating-to-cooling load ratio is approximately 2.5. Moreover, the seasonal thermal energy demand for air conditioning is equal to 15650 kWh and 1500 kWh during the heating and cooling periods, respectively, yielding a heating-to-cooling energy demand ratio of 10.4. These results highlight that building energy needs are strongly unbalanced between the seasons, with a significant predominance of the winter loads.

2.2. Hydronic distribution network and emitters

The considered HVAC system presents no night setback during the heating and cooling seasons. Five hydronic three-speed fan-coils are selected as terminal units and connected to the heat generator through a distribution loop based on a fixed-speed circulation pump. A 750 l thermal energy storage is installed in the distribution network to increase the system thermal inertia. The fan-coils are designed to cover the required load, considering an inlet water temperature of 45 °C during the heating season and 10 °C during the cooling season. Table 2 presents the main fan-coil technical data, in correspondence with the rated values of indoor air temperature (T_a), relative humidity (RH), inlet water temperature ($T_{w,in}$), a water temperature difference across the emitter of 5 K, and maximum fan speed.

2.3. Heat pump sizing and control system

To satisfy the building space heating and cooling demand, three different hydronic heat pumps were considered: (i) an Air-Source Heat Pump, ASHP; (ii) a Ground-Coupled Heat Pump, GCHP; (iii) a Dual-Source Heat Pump, DSHP. No additional backup systems are present because each HP is sized to cover the building peak load reported in the previous section. The DSHP can exploit either ambient air or the ground as external heat sources, selecting the most favorable option based on the adopted control strategy. The HP components technical specifications are reported in Table 3, while a comprehensive description of the unit and its main operating modes can be found in [29] and is not repeated here for the sake of brevity.

In order to compare the energy performance of each generator rigorously, the performance of the ASHP and GCHP is equivalent to that of the DSHP in air and ground modes, respectively. The nominal heating capacity in air mode is 11.4 kW, evaluated with an ambient air-dry bulb temperature of 7 °C. On the other hand, the nominal heating capacity in ground mode is 10.6 kW, assuming geothermal fluid inlet/outlet temperatures of 5 °C and 0 °C, respectively. In both cases, the inlet and outlet water temperatures at the load side are 40 °C and 45 °C, respectively. In Fig. 1, the DSHP heating/cooling capacity and *COP/EER* in both air-source and ground-source modes are reported as functions of the external source temperature (i.e., ambient air or borefield heat transfer fluid) and heat pump inverter frequency.

A PI controller is necessary to modulate the heat pump inverter frequency based on the load side water temperature at the thermal storage outlet. The PI control strategy is based on a hysteresis cycle, 5 K wide and centered on the reference value, set to 45 °C in winter and 10 °C in summer. When the minimum inverter frequency (30 Hz) is reached at low partial load, further modulation of the heat pump capacity becomes impossible, and on-off cycling is performed to meet the building thermal energy demand. To prevent compressor damage due to excessive on-off cycles, a minimum heat pump operating time of 10 min was implemented in the model, corresponding to a maximum frequency of 6 start-ups per hour, as recommended by the manufacturer. Moreover, both ASHP and DSHP in air-source mode employ the Reverse Cycle Defrosting (RCD) method [41] to melt the ice formed on the external surface of the evaporator during the heating season.

Table 2
Fan-coils technical data (reference conditions: T_a = 20 °C, $T_{w,in}$ = 45 °C in heating mode; T_a = 26 °C, RH 60%, $T_{w,in}$ = 10 °C in cooling mode).

Air flow rate in heating/cooling mode [$m^3\ h^{-1}$]	Water flow rate [$l\ h^{-1}$]	Heating capacity [W]	Cooling capacity [W]
319/233	256	1770	1380

Table 3
Technical specifications of the HP main components.

HP component	Technical specifications
Compressor	Scroll, model SNB172FEKMT (Siam)
Plate heat exchangers	24 plates Surface area 1.2 m^2 (Alfa Laval)
Finned coil heat exchanger	Fin space/thickness: 1.2 mm/0.1 mm Internal tube diameter 7.94 mm Surface front area 1.59 m^2 Design air flow rate 7104 $m^3\ h^{-1}$ (Eurocoil)
Electronic expansion valve	E2V24BSE (Carel)
Solenoid valve	HM4 (Castel)
Inverter	F003i-2PHB 13 A-HRFR01 (Frecon)
Refrigerant	R410A, charge 6.4 kg

2.4. Borehole heat exchanger field

For the GCHP and the DSHP in ground mode, another hydronic loop with a fixed-speed circulation pump connects the heat pump to a BHE field, based on double U-tube boreholes. The BHE pipes are made of high-density polyethylene, and a mixture of water and 25% Freezium is used as geothermal heat transfer fluid. Freezium is a commercial antifreeze fluid for BHEs that maintains low viscosity and high thermal conductivity at low temperatures [42,43]. The gap between the U-tubes and the soil is filled by a commercial sealant mortar (Termoplast Plus [44]). The main characteristics of the BHEs, such as borehole diameter (D_b), pipe internal and external diameter ($D_{p,i}$ and $D_{p,e}$), grout and pipe thermal conductivity (k_{gt} and k_p), shank spacing (s), ground thermal diffusivity and conductivity (α_{gnd} and k_{gnd}), and the main characteristics of the geothermal fluid, such as thermal conductivity (k_f), kinematic viscosity (ν_f), density (ρ_f) and freezing temperature (T_{ice}), are reported in Table 4.

The design length of the BHE field coupled to the heat pump (L_{nom}) was calculated according to the procedure reported by the ASHRAE [45], and its value is 150 m. Two inline boreholes, each 75 m in length, were considered. The linear thermal resistance for double U-tube pipes was evaluated with the analytical expression proposed by Lamarche et al. [46], obtaining a value of 0.09 m K W^{-1}.

2.5. Strategy for the selection of the optimal external source in the DSHP

The selection of the optimal external heat source is a crucial factor in maximizing the DSHP performance. In order to select the most favorable source (i.e., air or ground) during the heating season, three control strategies were investigated. To facilitate the application of the research findings, the investigated logics were selected considering the sensor equipment currently used in commercial units. The control logics considered in this paper are:

- Switching Temperature (ST) logic: when the external air temperature exceeds a reference value, identified as ST, the heat pump operates in air-source mode. Otherwise, it operates in ground-source mode. In

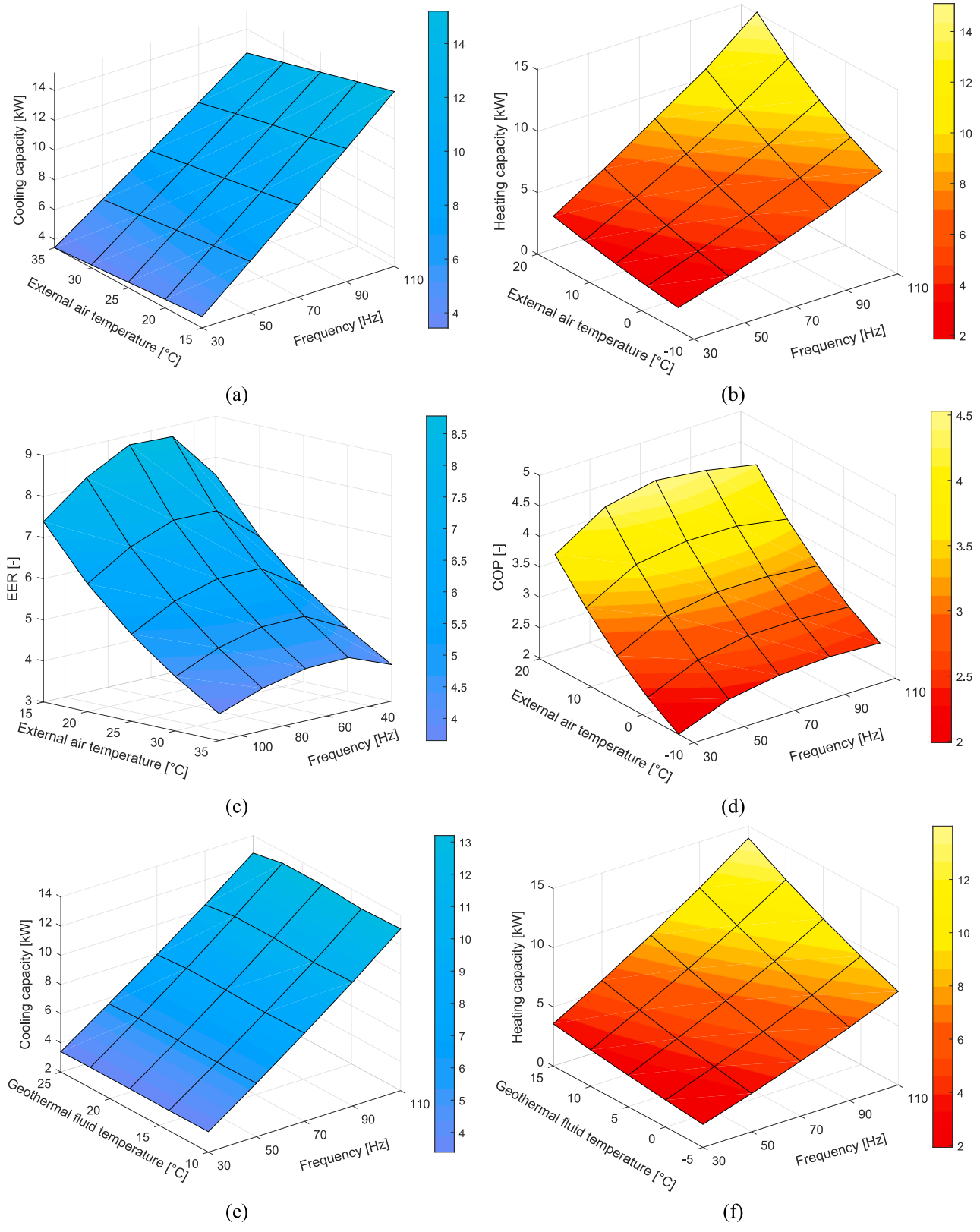

Fig. 1. Cooling and heating capacity, and *EER* and *COP*, for the DSHP in air-source mode (a-d) and ground-source mode (e-h) as functions of the external source temperature and heat pump inverter frequency (reference conditions: load side inlet/outlet water temperatures equal to 40/45 °C during the heating season and 15/10 °C during the cooling season).

this case, only a temperature sensor is needed to monitor the outdoor air temperature and control the DSHP operation.

- Sun Position (SP) logic: two daily time slots (nocturnal and diurnal) are identified, taking as boundaries the daily sunrise and sunset

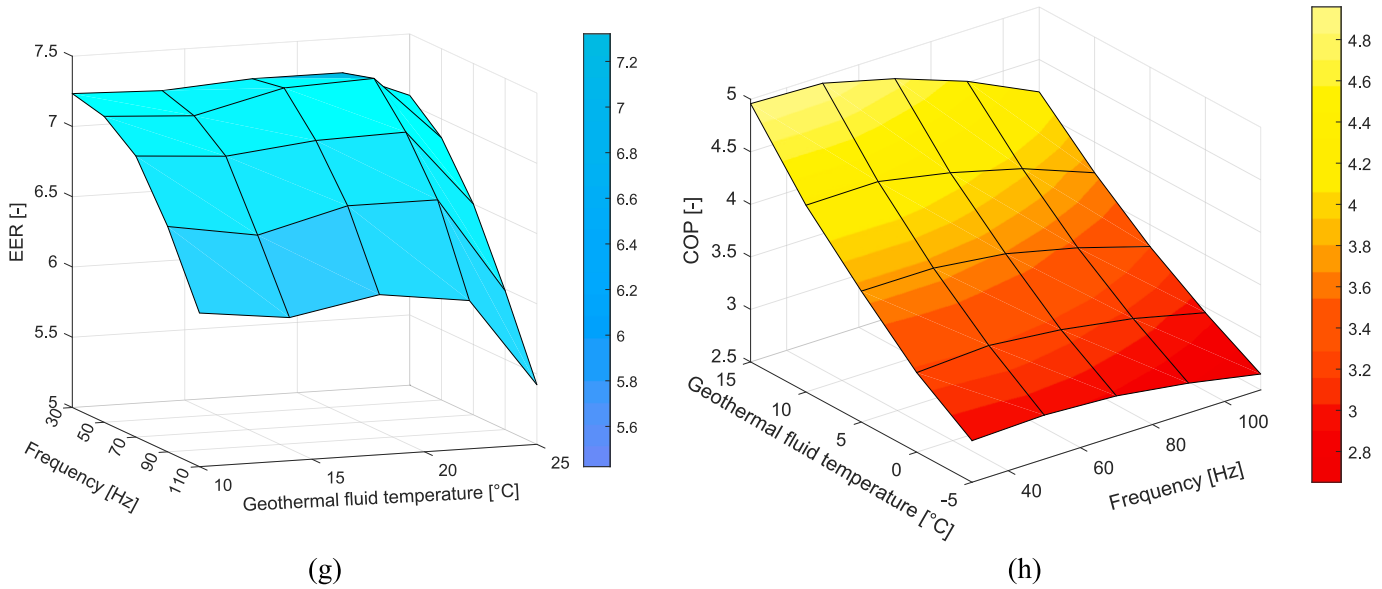

(g) (h)

Fig. 1. (*continued*).

Table 4
BHEs and geothermal fluid geometrical and thermophysical properties.

BHE geometrical and thermophysical properties							
D_b [cm]	$D_{p,i}$ [cm]	$D_{p,e}$ [cm]	s [cm]	α_{gnd} [m^2 s^{-1}]	k_{gnd} [W m^{-1} K^{-1}]	k_{gt} [W m^{-1} K^{-1}]	k_p [W m^{-1} K^{-1}]
15.2	2.6	3.2	8.3	8.56E-7	1.42	1.60	0.36
Geothermal fluid thermo-physical properties							
k_f^1 [W m^{-1} K^{-1}]	ν_f^1 [m^2 s^{-1}]		T_{ice} [°C]	ρ_f^1 [kg m^{-3}]			
0.50	2.65E-6		−20	1186			

Value evaluated at −5 °C.

times. During the diurnal hours, the heat pump exploits the aerothermal source; during the nocturnal hours, it deploys the geothermal source. To manage this control logic, only a clock is necessary.

- Predicted Coefficient of Performance (PCOP) logic: the DSHP operating mode is selected based on the highest instantaneous *COP* evaluated in air-source and ground-source modes. In particular, for the currently non-operating external source, the air/geothermal fluid temperature is continuously monitored, and the corresponding *COP* value is evaluated using the DSHP performance data; then, the most efficient external source is selected. In a real application, the PCOP logic is based on two sensors, needed to monitor the external sources temperature, and on the DSHP performance data, pre-loaded in the heat pump. To account for the energy losses associated with defrost cycles, the *COP* in air mode is reduced (i.e., multiplied by a penalty coefficient ranging between 0 and 1) during the heating operating mode when the outdoor air temperature is below 6 °C and the relative humidity is above 50%. The penalty coefficient in air mode ($1 - COP_{drop}$) is determined as described in Section 4.1. A summary of the PCOP logic is shown in Fig. 2. Due to the higher complexity of this control strategy, the DSHP performance data reported in Fig. 1 must be implemented within the heat pump controller as look-up tables.

As previously mentioned, the selected operation mode must be maintained for at least 10 min for each logic to prevent compressor damage from excessive switching between the two external sources. On the contrary, during the cooling season, the heat pump operates in ground-source mode only to partially recharge the ground due to strongly unbalanced building loads. This operation mode is applied to all control logics to avoid affecting relative comparisons.

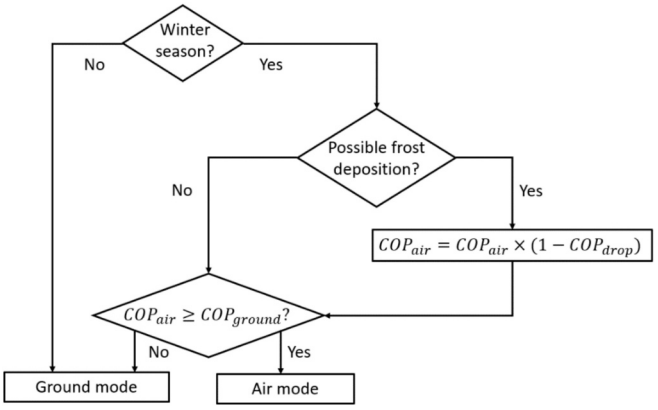

Fig. 2. PCOP logic flowchart.

2.6. Investigated HP configurations

In order to obtain a meaningful comparison among the different HP systems and evaluate the influence of the DSHP control logic on the heat pump seasonal energy efficiency, five different configurations were considered in this work. More specifically, in Cases A and B, the HVAC systems are based on conventional ASHPs and GCHPs, respectively. The other configurations present a DSHP in which the external heat source is selected according to the ST logic (Case C), the SP logic (Case D), or the PCOP logic (Case E). When the ground is exploited as the external source, four different borefield configurations were considered (subcases 1, 2, 3 and 4): 2 boreholes each 75 m long (100% of the design length), 1 borehole 125 m long (17% reduction), 1 borehole 100 m long

(34% reduction), 1 borehole 75 m long (50% reduction). For the sake of clarity, the configurations studied in this paper are presented in Table 5, and the corresponding schematic is shown in Fig. 3.

2.7. Key performance indicators

Long-term (10-year) simulations were carried out to investigate the performance of different heat pump systems and to assess the potential drift in the efficiency of the DSHP and GCHP over time due to an undersized borefield (subcases 2–4). The following seasonal and annual Key Performance Indicators (KPIs) [29] are considered to compare the system efficiency in each studied case:

$$SCOP_{net} = \frac{Q_h}{W_h} \quad (1)$$

$$SEER_{net} = \frac{Q_c}{W_c} \quad (2)$$

$$APF_{net} = \frac{Q_h + Q_c}{W_h + W_c} \quad (3)$$

The net Seasonal Coefficient of Performance ($SCOP_{net}$) is defined as the ratio between the thermal energy provided by the heat pump during winter (Q_h) and the electric energy (W_h) absorbed by the heat pump compressor and fans (the fans are employed by the ASHP and DSHP). Similarly, the Seasonal Energy Efficiency Ratio ($SEER_{net}$) is the ratio between the cooling energy provided by the heat pump during summer (Q_c) and the electric energy consumption throughout the same period (W_c). Finally, the net Annual Performance Factor (APF_{net}) accounts for the heat pump efficiency throughout the year and is defined as the ratio between the thermal energy supplied by the heat pump ($Q_h + Q_c$) and the absorbed electric energy ($W_h + W_c$).

3. Numerical model and validation

The presented HVAC system configurations were simulated by means of ALMABuild [38,39]. The numerical model was developed by using blocks from both the ALMABuild and Carnot (a toolbox extension developed for simulating the main HVAC system components [47]) libraries. More in detail, the models of the circulating pump and thermal storage were taken from Carnot. The building thermal zones were modeled using ALMABuild, while the numerical models of BHE field, DSHP, and controllers were developed specifically for this research. In Fig. 4, an extract of the Matlab-Simulink model is shown.

The Simulink variable-step solver ode23tb (stiff/TR-BDF2) was selected, utilizing an adaptive algorithm with the following settings: absolute and relative tolerances of 1E-2, and a time tolerance of 2.84E-13. The fluids thermo-physical properties, functions of pressure and temperature, are automatically updated at each time step. A scheme of the numerical procedure, showing the connections between the major simulation components, is shown in Fig. 5.

In order to demonstrate the accuracy of the developed numerical model, its main components, such as the building envelope and the HP and BHE field models, were validated by comparing results with those from the literature and the Carnot library, respectively.

3.1. Building thermal load validation

As described in Section 2.1, the modeled building is the SFH100 archetype developed by the IEA SHC Task 44 [36]. The building numerical model implemented in ALMABuild [38,39] is based on the RC formulation where thermal resistances and thermal capacitances simulate heat transfer within building envelope components and thermal zones. The numerical model was validated by locating the building in Strasbourg, the reference climate considered by the IEA SHC Task 44, and by imposing an internal air temperature of 20 °C during the heating season. According to IEA Task 44, the HVAC system is switched off from June to August. In Table 6, a comparison is presented between the monthly thermal energy demand of the SFH100 calculated using ALMABuild and obtained from the IEA Task 44.

Table 6 shows minimal differences across most months, with deviations not exceeding 3%. Only in February and October, the differences increase slightly, reaching about +6% and -12%, respectively. However, even in October, the absolute difference remains below 1 kWh m^{-2}. On an annual basis, the building thermal energy demand for space heating is nearly identical between the two approaches, differing by only 0.2%. Therefore, the building model can be considered validated.

3.2. Borehole heat exchanger field model validation

The numerical model of the BHE field developed in ALMABuild is based on the *g-functions* method proposed by Zanchini et al. [48]. According to this methodology, dimensionless thermal response functions simulate the trend in ground temperature produced by a uniform, constant dimensionless thermal load. The *g-functions* employed in this work assume the borehole as a finite-line-source [49] and the ground as a semi-infinite solid medium with constant thermo-physical properties, where no groundwater movement takes place; the presence of multiple boreholes is evaluated by applying the superposition of effects in space. After evaluating the borehole-ground interface temperature by means of *g-functions*, the BHE fluid outlet temperature can be calculated as a function of the instantaneous heat transfer rate with the ground and of the BHE linear thermal resistance [50].

The numerical results obtained with the numerical model developed in ALMABuild were compared to those achieved with the validated borefield model in the Carnot library. Both numerical models implement the *g-functions* method; however, in Carnot, the ground is split into a 'near probe' area with radial and axial nodes in a cylindrical geometry and a 'far probe' area, where the ground temperature is calculated using the Eskilson *g-functions* [51]. Moreover, the Carnot model has several limitations, including the requirement to use a 25% glycol solution as the geothermal fluid, the use of double U-tube boreholes, and a limited number of BHE field geometries. On the contrary, the borefield numerical model developed in ALMABuild can handle different geothermal fluids (e.g., water only, glycol solutions, Freezium solutions), various U-tube typologies (single or double), and a wider range of BHE field geometries. The numerical results obtained with the ALMABuild borefield model were compared with those yielded by the Carnot BHE field model by considering the same building-HVAC system described in Section 2.1. Due to the Carnot model constraints, a 25% glycol solution and double U-tube boreholes were simulated. Different borefield configurations (i.e., 1 BHE × 100 m, 2 BHEs×75 m and 2 BHEs×100 m) were considered for the validation. Table 7 presents the differences in annual and

Table 5
HP configurations analyzed.

	External source																
	Air (ASHP)	Ground (GCHP)/Air + Ground (DSHP)															
Borefield length [m]	–	150 (2 × 75 m)				125 (1 × 125 m)				100 (1 × 100 m)				75 (1 × 75 m)			
Source selection logic	–	–	ST	SP	PCOP	–	ST	SP	PCOP	–	ST	SP	PCOP	–	ST	SP	PCOP
Configuration	A	B1	C1	D1	E1	B2	C2	D2	E2	B3	C3	D3	E3	B4	C4	D4	E4

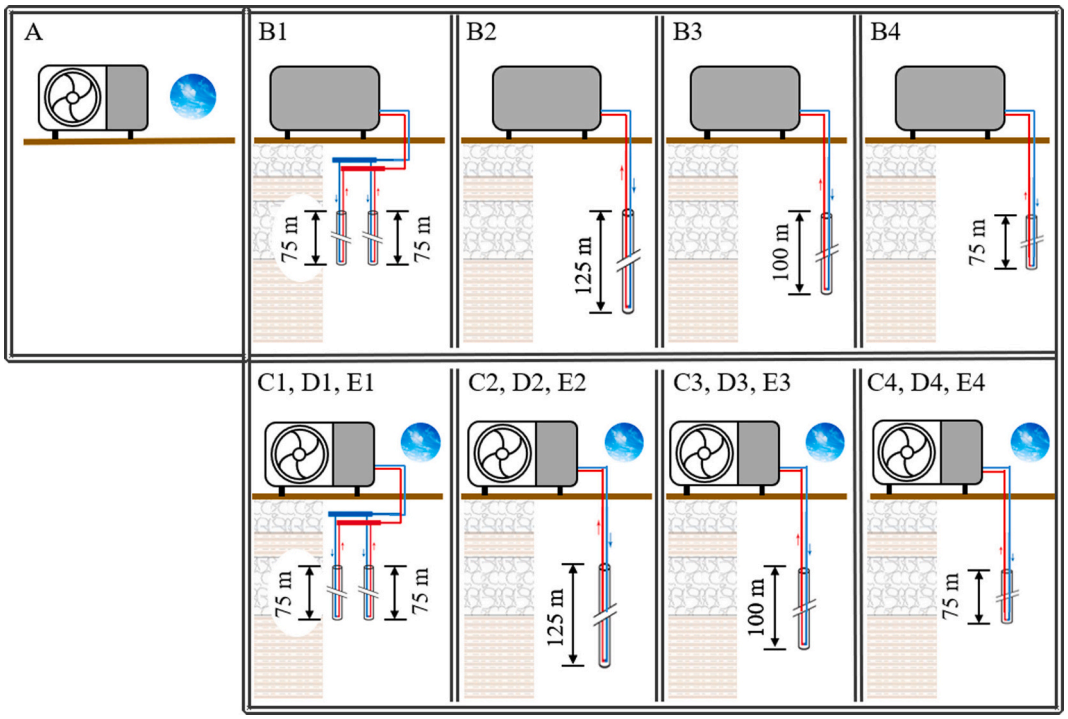

Fig. 3. Schematic of the different HP configurations.

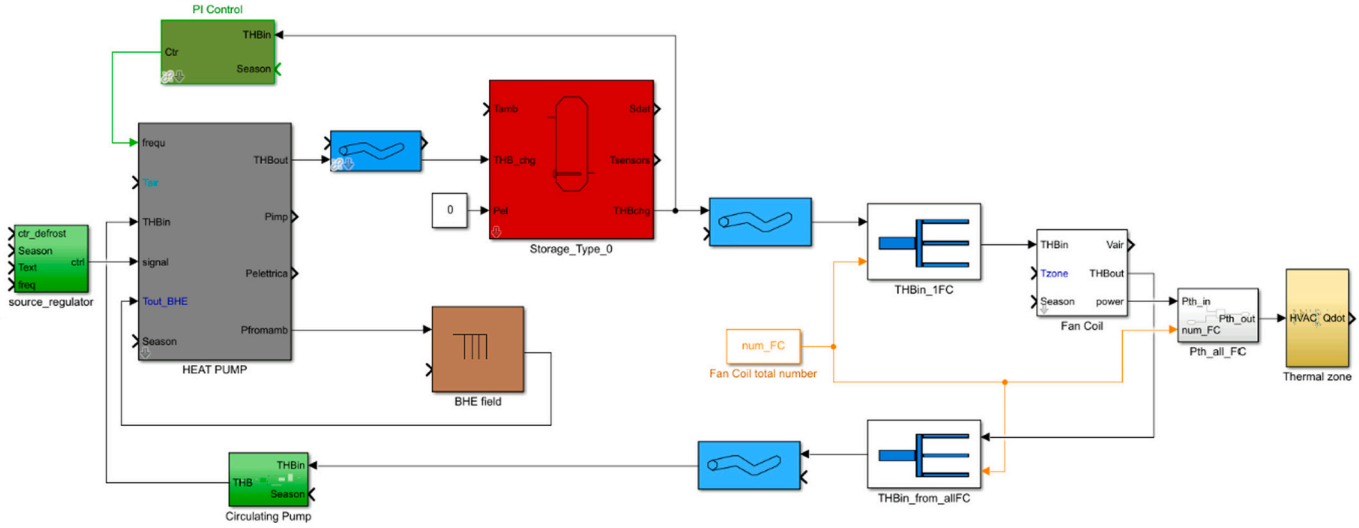

Fig. 4. Layout of the building-HVAC system numerical model developed in Simulink.

seasonal HP performance indicators and in the average geothermal fluid temperature at the BHE outlet ($T_{BHE,out}$) obtained using the ALMABuild model compared to the Carnot model.

The results reported in Table 7 suggest that, regardless of the BHE field configuration, the numerical results exhibit a steady trend after the fifth year of simulation, as evidenced by negligible and constant differences. The ALMABuild numerical model slightly underestimates the BHE fluid temperature at the borefield outlet compared to the Carnot model, and the deviation increases as the BHE size decreases. However, the maximum discrepancy is limited to 1 K (borefield 1 × 100 m) on an annual basis. Therefore, the energy performance of the HP coupled to the borefield is influenced marginally by the adopted model. The comparison of annual and seasonal HP performance indicators reveals that the maximum difference between the two models is approximately 3%.

3.3. HP model validation

The numerical models of the ASHP, GCHP, and DSHP developed in ALMABuild are based on the quasi-steady-state performance data provided by the manufacturer (reported in Fig. 1), implemented using the Lookup Table Simulink block. More in detail, linear interpolation/extrapolation is applied to calculate the HP performance for working conditions within/outside the input dataset. The developed models take into account elements typically not considered by simulation software, such as the internal thermal inertia linked to the water volume in the HP piping (5 l) and heat losses to the ambient air (0.3 W K^{-1}), as well as the HP dynamic behavior during on-off cycling. Experimental tests were carried out on the DSHP prototype to characterize the energy losses associated with on-off cycles. According to the methodology described in [29], four numerical parameters were obtained. Two coefficients, γ

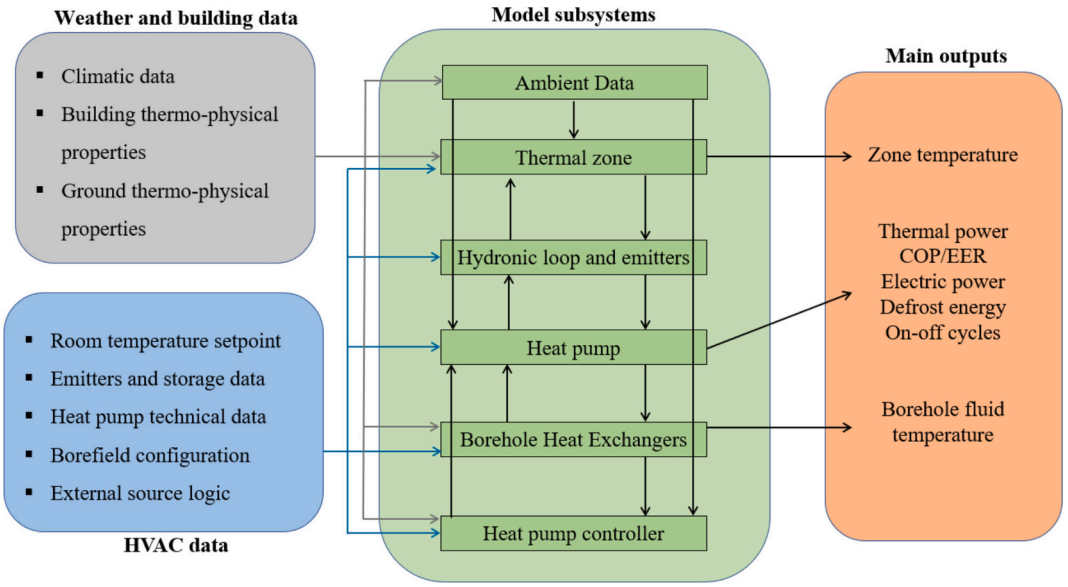

Fig. 5. Scheme of the numerical model, with connections between the simulated components, input data and main outputs.

Table 6
Comparison of SFH100 thermal energy demand obtained by ALMABuild and IEA Task 44.

	ALMABuild [kWh m^{-2}]	IEA Task 44 [kWh m^{-2}]	Difference [%]
January	21.9	22.8	−3.9
February	17.6	16.6	+5.9
March	11.3	10.9	+3.0
April	4.7	4.8	−2.5
May	1.0	1.0	−0.2
September	0.8	0.8	−2.9
October	5.4	6.1	−12.1
November	15.2	15.5	−2.4
December	21.7	21.1	+3.0
Total	99.5	99.7	−0.2

and β, were related to the reduction of the heat pump capacity and electric power input during the start-up phase, respectively. The duration of the transients related to the heat pump capacity and absorbed electric power (τ_γ and τ_β, respectively) was also determined. The values of these numerical parameters affecting HP performance during the start-up transients are reported in Table 8.

Moreover, both ASHP and DSHP in air-source mode must perform periodic defrost cycles during the heating season following the RCD method [41]. In the numerical model, a defrost cycle is activated when the outdoor air temperature is below 6 °C and the ambient relative humidity is above 50% for at least 10 min [52]. According to [52], three subsequent phases were modeled: (i) an initial phase having a duration τ_1, in which the heat pump is switched off; (ii) an intermediate phase with a duration τ_2, during which the cycle is inverted and the heat pump operates in cooling mode with cooling capacity P_c and Energy Efficiency Ratio EER_c; (iii) a final phase having a duration τ_3, in which the heat pump is switched off again. In Table 8, the values of these parameters characterizing the defrosting transients are reported. The minimum interval between two consecutive defrost cycles is one hour.

The HP model was validated by comparing its results with those of the validated Carnot HP model. In the utilized version of Carnot (7.3), the numerical model of a fluid-to-fluid heat pump is included. In particular, the HP performance data, such as heating capacity and absorbed electric power, are modeled using linear functions of the sink/source temperatures [53], meaning that the HP *COP/EER* does not change with partial load factor. Moreover, in the Carnot HP block, no efficiency losses related to on-off cycling or defrost cycles are considered.

For validation purposes, two numerical simulations were conducted using both tools, employing the same building-HVAC system described in Sections 2.1–2.3 for the heating season. Since models of air-to-water units are missing in Carnot 7.3, the heat pump was operated in geothermal mode to consider operating conditions as close as possible.

The simulation results indicate that both approaches yield nearly identical seasonal performance during the heating season, with a $SCOP_{net}$ value equal to 2.94. Furthermore, Fig. 6 illustrates the HP heating capacity, evaluated through both tools, over 200 h of the season (from November 25th to December 2nd). The obtained numerical results confirm the excellent agreement between the two tools.

Table 8
Values of the parameters characterizing the defrost cycles and cycling losses.

Defrost cycle					On-off cycle			
P_c [kW]	EER_c	τ_1 [s]	τ_2 [s]	τ_3 [s]	γ	β	τ_γ [s]	τ_β [s]
−11.4	6	30	360	30	0.69	0.96	216	78

Table 7
Validation of the BHE model for different borefield configurations: relative difference in the outlet geothermal fluid temperature and in the annual and seasonal HP performance.

	1 × 100 m (65% L_{nom})				2 × 75 m (L_{nom})				2 × 100 m (135% L_{nom})			
	$T_{BHE,out}$	APF_{net}	$SCOP_{net}$	$SEER_{net}$	T_{BHEout}	APF_{net}	$SCOP_{net}$	$SEER_{net}$	$T_{BHE,out}$	APF_{net}	$SCOP_{net}$	$SEER_{net}$
Year	Δ [K]		Δ [%]		Δ [K]		Δ [%]		Δ [K]		Δ [%]	
1	−0.5	+0.8	+0.7	+2.6	−0.2	−1.5	−1.6	+0.1	−0.2	−1.5	−1.6	+0.1
5	−1	−0.3	−0.5	+3.2	−0.6	−2.5	−2.8	+0.1	−0.6	−2.5	−2.8	+0.1
10	−1	−0.3	−0.6	+3.2	−0.7	−2.6	−2.9	0	−0.7	−2.6	−2.9	0

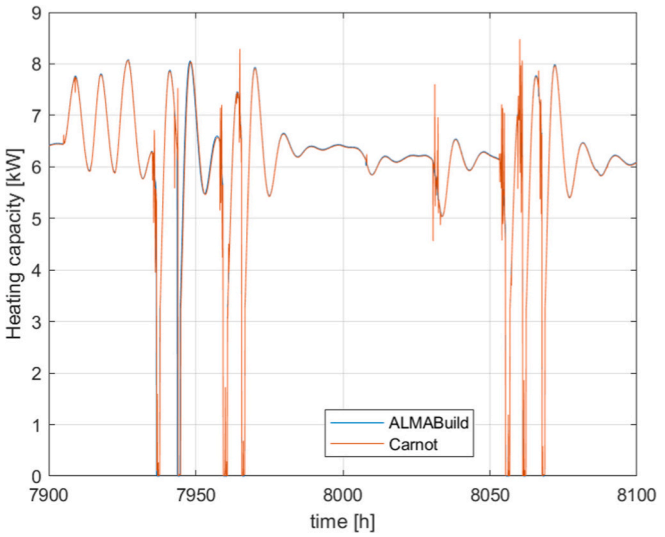

Fig. 6. Comparison between the HP heating capacity evaluated by means of ALMABuild and Carnot.

4. Results and discussion

The following Sections report the main results of the case studies analyzed in this paper (summarized in Table 5). Since selecting the optimal heat source is crucial to maximizing DSHP performance, the numerical results demonstrate the impact of DSHP control logics on seasonal and annual energy efficiency.

4.1. Case A

In configuration A, the HVAC system is based on an ASHP. The unit has the lowest seasonal efficiency during the winter season, with a $SCOP_{net}$ value of 2.50. Conversely, the value of $SEER_{net}$ is equal to 4.50, about 80% higher than that of $SCOP_{net}$. The APF_{net} is equal to 2.67, close to the $SCOP_{net}$ value due to unbalanced building loads.

The numerical results show that the HP seasonal energy performance is dramatically influenced by the high cycling frequency: the unit performs 2090 cycles throughout the year, almost entirely clustered during the heating season (1922 cycles in winter and only 168 in summer). This outcome is mainly due to the high frequency of defrosting cycles, higher than 8 per day. This characteristic becomes even more pronounced during the most severe part of the winter, from December to January, when the daily number of defrost cycles increases by more than 50% (to 17 per day).

To investigate the influence of the ASHP defrosting cycles on the seasonal performance factor, an additional simulation was carried out, neglecting frost deposition on the HP evaporator and, consequently, the energy losses associated with the frosting phenomenon. On the contrary, the penalization due to on-off cycles was still taken into account. The numerical results show that the $SCOP_{net}$ could increase by 24% if energy losses associated with defrosting cycles were not considered.

Since defrost cycles significantly influence ASHP seasonal performance, it is worthwhile to display the HP hourly performance during these transients. In this regard, Fig. 7 shows the ASHP heating and cooling capacity during three typical hours of the heating season.

During the selected interval, consecutive defrost cycles occur every hour. Accordingly, two hourly time intervals can be defined: the first one starts when the ASHP reverses the cycle (RCD period), accounting for the energy losses due to the defrost cycle, and the second one is placed between two consecutive defrost cycles (*und*, undisturbed period), accounting for the stationary ASHP performance. For each interval, the hourly *COP* is calculated as the ratio of the thermal energy supplied by the HP and the electric energy absorbed by the HP during that period.

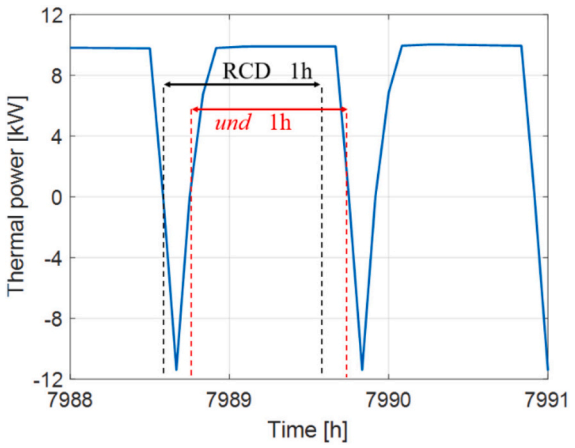

Fig. 7. ASHP heating (positive values) and cooling (negative values) capacity during three hours in winter with defrost cycles.

Consequently, an hourly *COP* drop due to the defrost transient can be determined as follows:

$$COP_{drop} = \frac{COP_{und} - COP_{RCD}}{COP_{und}} \quad (4)$$

In Fig. 8, the COP_{drop} values obtained during the heating season are shown as a function of the external air temperature. As shown in the Figure, the *COP* drop is linearly influenced by the external air temperature; the higher the ambient temperature, the lower the penalty. Generally, the hourly drop ranges from 30 to 35% when the external air temperature decreases from 6 to −2 °C. The hourly *COP* penalization is strongly correlated to the heat pump defrosting technique. In the literature, the hourly *COP* degradation due to reverse cycle defrosting (RCD) is estimated to be between 20% and 40% [41,54]; consequently, the results obtained here are consistent with this range. A COP_{drop} value equal to 0.3 was incorporated into the PCOP logic of the DSHP to account for the impact of defrost cycles.

4.2. Case B

In Case B, the GCHP is coupled to different BHE field configurations (see Table 5), ranging from a minimum length of 75 m (Case B4, 50% undersizing) to the design borefield size of 150 m (Case B1). Table 9 reports the HP seasonal and annual performance factors achieved in a long-term horizon (up to 10 years).

As shown in Table 9, the highest efficiency can be achieved with the

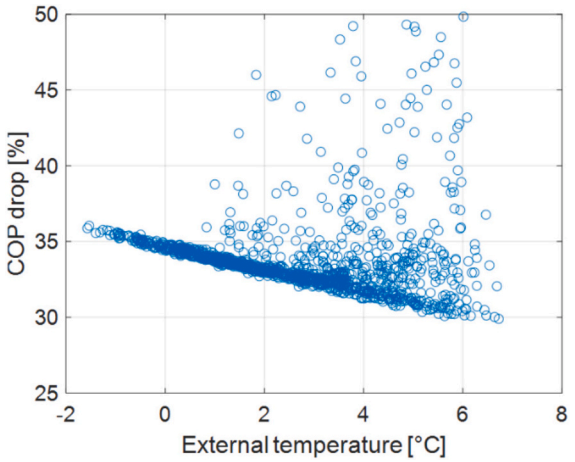

Fig. 8. *COP* penalization due to defrost cycles as a function of the external temperature.

Table 9
Seasonal and annual performance factors of the GCHP.

Year	B1			B2			B3			B4		
	$SCOP_{net}$	$SEER_{net}$	APF_{net}	$SCOP_{net}$	$SEER_{net}$	APF_{net}	$SCOP_{net}$	$SEER_{net}$	APF_{net}	$SCOP_{net}$	$SEER_{net}$	APF_{net}
1	3.43	6.78	3.69	3.32	6.74	3.58	3.08	6.54	3.34	2.76	6.10	3.00
5	3.36	6.80	3.62	3.27	6.76	3.53	3.04	6.59	3.30	2.72	6.17	2.96
10	3.33	6.81	3.60	3.25	6.77	3.52	3.02	6.61	3.28	2.70	6.20	2.94

design configuration B1 with values of $SCOP_{net}$, $SEER_{net}$ and APF_{net} at the tenth year equal to 3.33, 6.81 and 3.60, respectively. Moreover, it is noted that in summer the system operates at high efficiency, even with configuration B4, based on the shortest borefield. Due to the low energy demand during the cooling season, the reduction in $SEER_{net}$ is limited to 10% compared to Case B1. On the other hand, the values of $SCOP_{net}$ and APF_{net} exhibit a more significant penalty as the borefield size decreases. In detail, the $SCOP_{net}$ drop in relation to Case B1 ranges from −5% (B2) to −21% (B4). A similar penalty is observed for the APF_{net} with a maximum reduction of 18% for configuration B4. Throughout the 10-year simulation period, the APF_{net} closely mirrors the trend observed for the $SCOP_{net}$, exhibiting a slight reduction of approximately 2–3% by the end of the decade. This decline is primarily attributed to the ground thermal drift, which manifests as a gradual decrease in the geothermal fluid temperature during the heating season (i.e., the season with the highest loads). Specifically, the mean fluid temperature decreases from 4.8 °C to 3.7 °C in Case B1 and from −2.7 °C to −3.5 °C in Case B4, highlighting the long-term impact of ground thermal imbalance on the system performance.

The HP electric consumption in Case B1 is about 5350 kWh y^{-1} in the first year and increases by 150 kWh (+3%) over the simulated period. Conversely, the reduced efficiency of the heat pump in Case B4 results in higher electric consumption: 6610 kWh in the first year, followed by a more modest increase of approximately 100 kWh over the long term (+1.5%). The energy demand associated with the circulating pump of the geothermal loop is approximately 66 kWh y^{-1}, about 1% of the total.

Comparing Cases B1 and A, it is noted that the thermal energy supplied by the GCHP during the heating season is much lower (−7.5%, −1380 kWh), as well as the corresponding electric consumption (−23%, −1450 kWh). Although the air unit delivers more energy to the heating system, the RCD technique reduces the amount of thermal energy effectively available to the building.

The frequency of the heat pump on-off cycling is stable throughout the years in both heating and cooling operating modes. During winter, the GCHP coupled to the design borefield performs about 270 start-ups, with an average of about 1.5 cycles per day. During the cooling season, the daily cycling frequency increases to approximately 2.9 due to the heat pump being oversized relative to the cooling load. A slight reduction in the number of on-off cycles performed by the GCHP is observed during the heating season in Case B4, due to the undersized borefield, which lowers the heat pump capacity.

4.3. Case C

In Cases C1-C4, the heat generator is the DSHP described previously. During the heating season, the external source is selected based on the switching temperature (ST) logic (see Section 2.5). On the other hand, during the cooling season, the DSHP operates in ground-source mode only, partially recharging the soil and exploiting a more efficient sink than the external air.

Fig. 9 shows the APF_{net} trend over the 10-year simulation period as a function of the switching temperature, for the different BHE field configurations. It is worth highlighting that a DSHP working with a switching temperature value of 26 °C operates in ground-source mode only, achieving the same performance as the GCHP coupled with the same borefield. It can be observed that the APF_{net} increases for a given switching temperature and simulation year, ranging from Case C4 to Case C1. Indeed, the higher the total BHE length, the better the heat pump energy performance, due to more favorable ground temperatures.

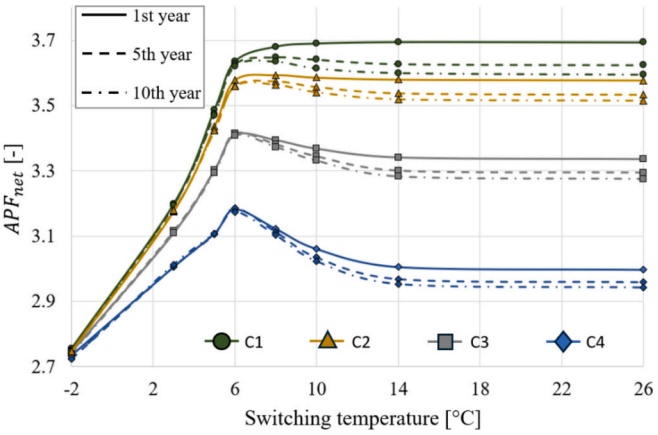

Fig. 9. APF_{net} values obtained in Case C as a function of the borefield configuration and the time horizon.

Another important outcome is that an optimal switching temperature, which maximizes the APF_{net} value, can be found for a fixed BHE length. In particular, this value increases as the borefield size rises: in Cases C3 and C4 (33% and 50% of undersizing, respectively), the optimal switching temperature value ST is 6 °C at the tenth year, whereas in Cases C2 and C1 (17% and 0% of undersizing, respectively) it increases up to 8 °C (see the dot-dash curves in Fig. 9). This trend is coherent: the ground utilization is prolonged with higher values of the switching temperature, and, with a borefield not much undersized, the DSHP guarantees better energy performance in ground-source mode than in air-source mode. In other words, with a shorter borefield, the geothermal fluid temperature decreases faster, leading to worse heat pump performance in ground mode. As a consequence, the period of the winter season in which the heat pump COP in air mode would be higher than that in ground mode is longer if a shorter borefield is adopted. In this case, a lower switching temperature, which maximizes the exploitation of the air source and reduces that of the ground, results in a higher APF_{net}. It is worth noting that defrost cycles can be avoided if a ST value above 6 °C is set. In general, values of ST lower than 6 °C must be discarded for twofold reasons: (i) prolonged operation of the DSHP in air-source mode in correspondence of not favorable conditions (low external air temperature); (ii) energy losses linked to defrost cycles, occurring with low air temperatures.

It can be observed that the APF_{net} remains almost constant over the years, for all BHE field configurations, particularly for very low values of the switching temperature. Indeed, with a ST value of −2 °C, almost no thermal energy is extracted from the soil in winter and, therefore, no ground temperature drift occurs with the undersized borefields to penalize the $SCOP_{net}$ value. Additionally, during the summer, the thermal energy transferred to the ground is insufficient to significantly increase its temperature, due to the low building loads; thus, no penalty to the $SEER_{net}$ values is observed with undersized borefields. Both these aspects translate into annual performance independent of the year for each BHE field size, at low ST values. On the contrary, for a given borefield size and with ST values larger than 6 °C, the DSHP annual

performance decreases over the years due to the thermal drift of the ground. The higher the switching temperature, the longer the time spent with the DSHP in ground mode, and the greater the penalty on the APF_{net} due to the soil temperature decrease.

By considering the 10th-year results of Case C4, it can be outlined that the adoption of an optimized switching temperature (i.e., $ST = 6$ °C) in the presence of an undersized BHE field allows for achieving an increase in the APF_{net} value up to 8% compared to a conventional GCHP coupled with the same borefield (compare the APF_{net} values reached by the blue dot-dash curve in correspondence of $ST = 6$ °C and $ST = 26$ °C). This improvement is related to the deployment of external air as the heat source for a significant share of the heating season, allowing the soil to restore its undisturbed temperature partially when the DSHP operates in air-source mode. In addition, an examination of the 10th-year results for Case C1 demonstrates that setting the optimized switching temperature (8 °C) yields an APF_{net} value slightly higher than that of the conventional GCHP system ($ST = 26$ °C). In summary, the efficiency improvement achievable after 10 years by a DSHP implementing an optimized switching temperature ranges from 1% (C1) to 8% (C4) compared to a conventional GCHP operating with a borefield of equal length.

4.4. Case D

In configuration D, the DSHP uses the sun position (SP) logic as the source control strategy during the heating season. The APF_{net} values achieved with this control logic are shown in Fig. 10.

The numerical results show that the larger the BHE field size, the higher the APF_{net} value, in agreement with the outcomes of the previous control logic. The minimum and maximum values of APF_{net} at the tenth year are 3.08 and 3.42, respectively, for Cases D4 and D1. The system efficiency remains almost stable over the 10-year horizon for a given BHE length. Thus, even with the SP logic, it is possible to limit the ground temperature drift caused by undersized borehole fields: the ground temperature can be restored, even with building thermal loads significantly unbalanced throughout the year, because part of the heating load is covered in air-source mode.

The annual number of defrost cycles (approximately 550) remains constant regardless of BHE size or the passage of time, as the DSHP utilizes external air as the heat source according to a time-scheduling logic. Consequently, in each configuration, the DSHP operates in air-source mode for the same period, and the frequency of defrost cycles depends solely on ambient climatic conditions (which repeat each year according to the TRY). Since it is not possible to completely avoid frosting, the SP logic is recommended only for mild climates.

4.5. Case E

In configuration E, the DSHP operates according to the predicted *COP* (PCOP) logic, which selects the most favorable external source on the basis of the highest value of the instantaneous *COP*. The instantaneous *COP* is evaluated for air- and ground-source modes every 10 min and, according to the study of the ASHP performance during defrost cycles reported in Section 4.1, a COP_{drop} value of 0.3 is considered for the air-source mode when the external air temperature is lower than 6 °C and the *RH* is higher than 50%.

Fig. 11 shows the seasonal and annual performance figures of the DSHP operated with the PCOP logic, for the tenth year for each configuration. The $SEER_{net}$ is slightly influenced by the borefield size, with values ranging between 6.14 (Case E4) and 6.8 (Case E1), corresponding to a span of approximately 11%. It is noteworthy that the DSHP energy performance during the cooling season is up to 50% higher than that yielded by a conventional ASHP ($SEER_{net} = 6.8$ in Case E1 versus $SEER_{net} = 4.50$ in Case A). On the other hand, the DSHP exhibits lower efficiency in heating mode than in cooling mode. The $SCOP_{net}$ varies from 2.92 to 3.39, increasing the total borefield length from 75 to 150 m. However, the $SCOP_{net}$ values are still higher than that achieved by the ASHP (2.50) even with undersized borefields.

The numerical results confirm that higher APF_{net} values can be obtained for longer borefields. This outcome is further investigated in Fig. 12a, which illustrates, for the tenth year of operation, the cumulative frequency of the geothermal fluid temperature entering the DSHP when it operates in ground-source mode. The reported data indicate that the borefield size significantly influences the BHE fluid inlet temperature. During the winter season, for the shortest field configuration (E4), the DSHP operates for approximately 40% of the time with values of the geothermal fluid at the DSHP inlet ranging between −9.6 and − 2.6 °C. In contrast, for the longest configuration (E1), for 40% of the time, the BHE fluid temperature is higher (between −0.8 and 3.8 °C).

Fig. 12b presents the cumulative frequency of the external air temperature values when the DSHP operates in air-source mode during winter. A marked discontinuity is evident around 6 °C, attributed to the penalty factor applied to the heat pump *COP* when the ambient conditions are favorable for frost formation. Consequently, the DSHP works in air-source mode less than 5% of the time when the external air temperature falls below 6 °C, regardless of the BHE field size. For values of the external air temperature above 6 °C, the cumulative frequency pattern remains similar across the different configurations. It is worth noting that, even though for the ST logic the switching temperature that maximizes the performance is generally above 6 °C, under the PCOP logic a fixed temperature threshold is not defined. In the latter case, the heat pump is seldom operated in air mode with low values of the outdoor temperature due to the *COP* penalty factor, which accounts for the potential occurrence of defrosting cycles.

Another parameter worth investigating is the temperature difference between the ground and air when the controller determines the most favorable external source. Some authors used this parameter to identify

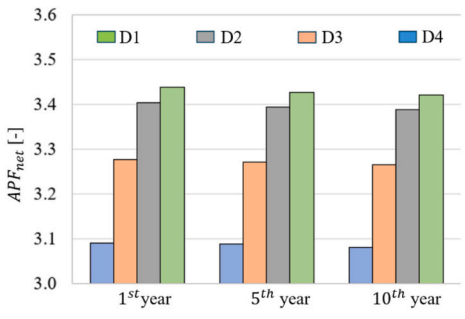

Fig. 10. APF_{net} values obtained in Cases D.

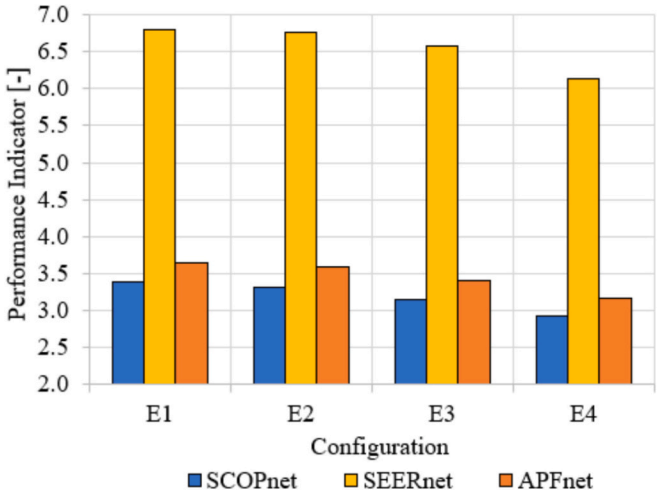

Fig. 11. DSHP seasonal and annual performance indicators obtained in Case E at the tenth year.

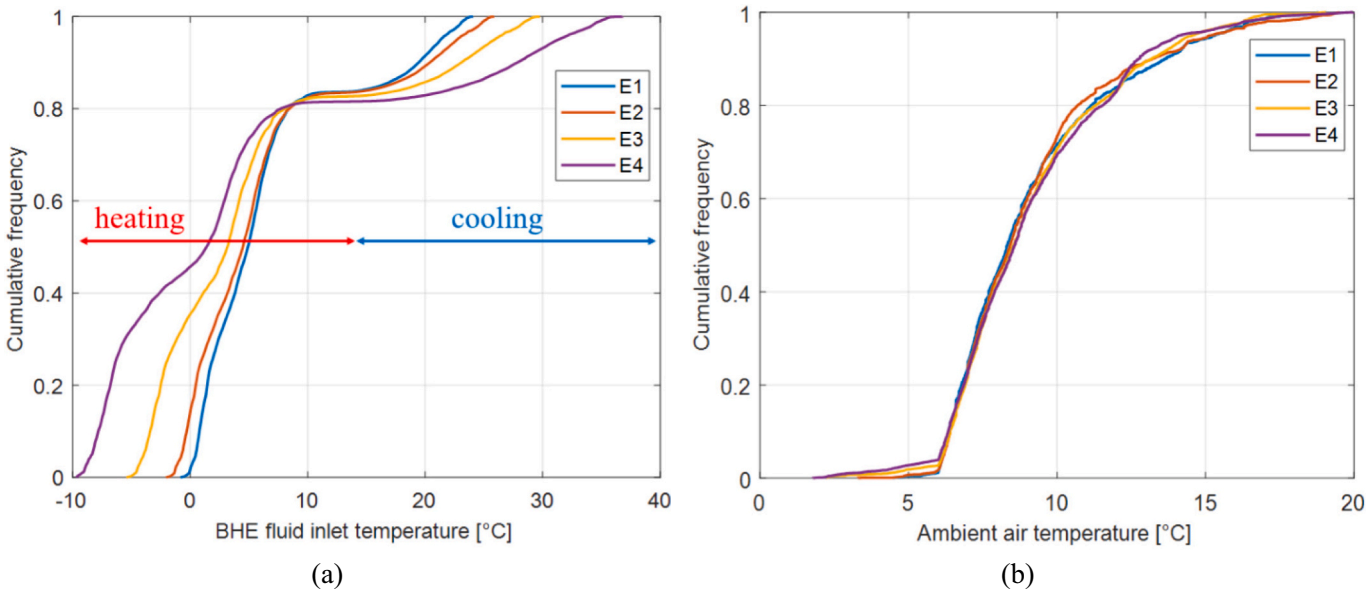

Fig. 12. Cumulative frequency of the BHE fluid inlet temperature (a) and outdoor air temperature (b) when the DSHP operates in ground- and air-source modes, respectively (10th year of operation).

the optimal source for the DSHP operation [17,19,31,55]. Fig. 13 illustrates, on a weekly basis, the temperature difference between the selected external source and the other one during the tenth heating season, when the DSHP transitions from ground-source mode to air-source mode (ΔT_{air} in red) and vice versa (ΔT_{gnd} in blue). In particular, the graph shows the average, maximum and minimum value of the temperature difference, as well as the switch frequency. For the sake of clarity, positive/negative values of this parameter indicate that the selected external source is hotter/colder than the other one.

From the comparison of Figs. 13a (configuration E1) and 13b (configuration E4), it is evident that the switch frequency for the heating operating mode in configuration E4 is significantly higher than that in configuration E1. Indeed, with the shortest borefield configuration, the ground temperature exhibits more rapid variations, leading to a more frequent switch between the two external sources (1687 switches for configuration E4 compared to 559 for configuration E1). The average values of ΔT_{air} and ΔT_{gnd} are equal to 7 °C and − 5.6 °C in configuration E4, respectively, and 5.3 °C and − 4.3 °C in configuration E1, respectively. Consequently, on average, the *COP* in air mode exceeds that in ground mode only when the external air temperature is 5–7 K higher than that of the geothermal fluid. Even higher ΔT_{air} values can occur when the penalty coefficient (1–COP_{drop}) applies (see Dec–Feb period in Fig. 13b). These numerical results highlight that selecting the external source based on a fixed temperature difference does not allow to optimize the heat pump energy performance, since the optimal value depends on the borefield size. In contrast, the PCOP logic, based on the higher instantaneous *COP*, allows the selection of the optimal external source, accounting for variable temperature differences throughout the season.

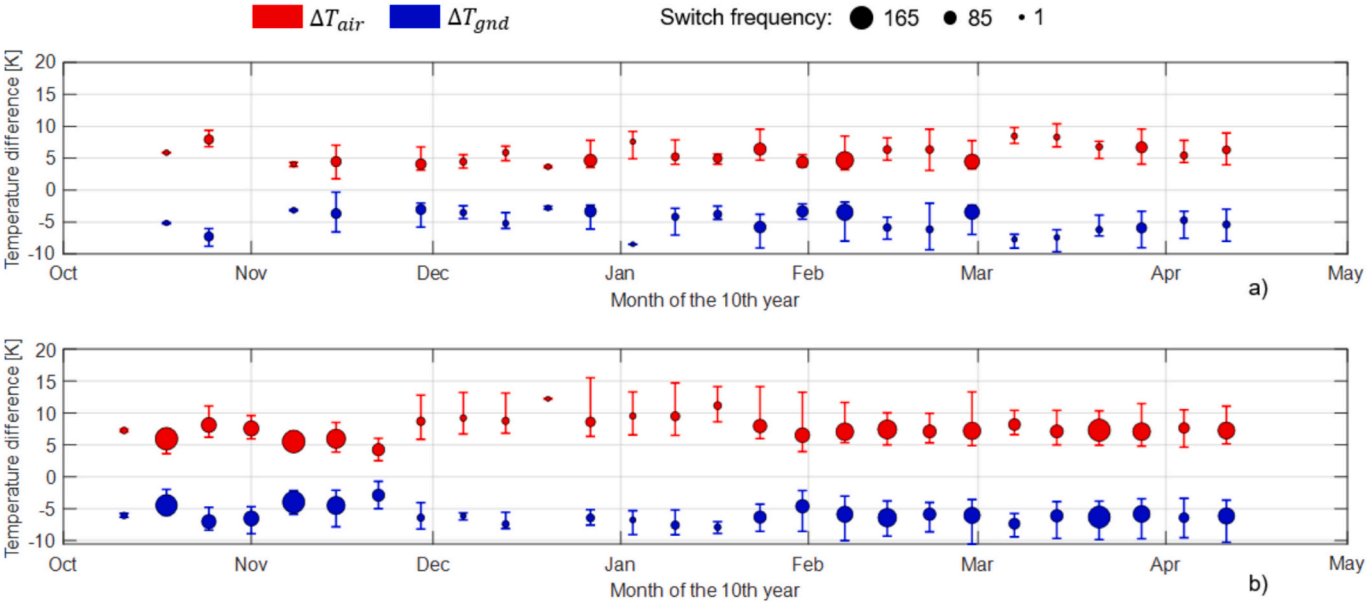

Fig. 13. Weekly average, maximum and minimum temperature difference between the two external sources when the controller determines the most favorable one for configurations E1 (a) and E4 (b), during the tenth heating season; switch frequency is represented by circle size.

4.6. Discussion

This Section presents a global comparison of the annual performance across the different cases analyzed. Table 10 shows, with reference to the tenth year of simulation, the performance parameters for all the analyzed cases. In particular, the annual values of heat absorbed by the heat pump from the two external sources (air or ground), the share of the building energy demand covered in aerothermal and geothermal mode, the heat pump electric energy consumption, and the $SCOP_{net}$, $SEER_{net}$ and APF_{net} are presented as a function of heat pump typology (ASHP, GCHP, DSHP), borefield size (1–4) and control strategy (C-E). For clarity, heat exchanged with external sources is assumed negative in cooling mode (i.e., during RCD and summer season) and positive in heating mode. It is important to highlight that the results presented for the ST logic (cases C1-C4) are obtained by selecting the optimal switching temperature, which varies for each BHE field size (see Section 4.3).

The results in Table 10 clearly show that the ASHP achieves the worst energy performance, with the highest electric energy consumption (7318 kWh) and the lowest KPI values. Moreover, when ground is used as the heat source, the shorter the borefield, the lower the average geothermal fluid temperature and energy extracted from the ground, resulting in higher electric consumption. For instance, the geothermal and electric energy contributions in case B1 are 8565 kWh and 5488 kWh, respectively, whereas the corresponding values in case B4 are 7354 kWh (−14%) and 6709 kWh (+22%), respectively. In cases D1-D4, the BHE size does not affect the aerothermal energy share (below 30% of the overall building energy demand), since it depends on the number of hours operated in air-mode, which is determined by the SP logic and does not change with the BHE size. Generally, the DSHP operation reduces geothermal energy usage compared to a traditional GCHP, from 5% (case E1) to 32% (Case C4). The $SEER_{net}$ values are twice those of the corresponding $SCOP_{net}$ values due to reduced cooling building demand, making even the shortest BHE field configuration a favorable heat source. The APF_{net} value always follows that of the $SCOP_{net}$ due to the significant unbalance in building loads.

A comparative analysis was conducted with the study presented in Ref. [29], which investigates a building of analogous size located in a similar climatic context and equipped with the same HP typologies. With regard to the DSHP operation, the optimization procedure identified the same optimal switching temperature (6 °C) under the ST control logic, assuming a 50% reduction in borefield size. The resulting annual energy shares between aerothermal and geothermal sources are 32% and 68% in the present study, compared to 40% and 60% reported in [29]. Furthermore, the overall *APF* achieved by the DSHP system is comparable between the two studies, with a value of 3.17 obtained in this work and 3.13 found in [29].

Fig. 14 focuses particularly on the APF_{net} values obtained in the tenth year of simulation in each studied case.

The APF_{net} of the conventional GCHP coupled with the design BHE field (Case B1), equal to 3.60, is marked as the reference case. As shown in Fig. 14, the dashed horizontal line indicates that the ASHP achieves the lowest performance, yielding an APF_{net} of 2.67. Conversely, when the heat pump exploits the ground as the external heat source, either as a GCHP or a DSHP, the system performance increases significantly, ranging from a minimum improvement of 10% (GCHP, Case B4) to a maximum of 37% (DSHP, Case E1). More in detail, for a GCHP connected to a BHE field with the nominal length, the value of APF_{net} is 3.60 (see the reference case in Fig. 14). Interestingly, a slightly higher performance can be achieved by the DSHP connected to the same design borefield. Indeed, Cases C1 and E1 achieve the highest performance indicators among all the studied cases, because the DSHP is coupled to the design borefield (nominal length) and can efficiently exploit external air when more convenient than ground through the ST or PCOP logics (APF_{net} equal to 3.64 for Case C1 and to 3.65 for Case E1). With the ST and PCOP logics, using a DSHP coupled to an undersized (and, thus, more economical) borefield can even yield about the same annual performance as that of the GCHP with the design borefield (Cases C2 and E2: L_{nom} – 17%, APF_{net} − 1% than the reference case), or slightly lower (Cases C3 and E3: L_{nom} – 34%, APF_{net} − 5% than the reference case).

For a given strongly undersized borefield, the DSHP APF_{net} is always higher or at least comparable to that of the GCHP, regardless of the adopted control logic (compare Cases C-E4 to Case B4). Nevertheless, in general, the logic for selecting an external source strongly influences achievable performance: although a DSHP can outperform a GCHP in most scenarios, this potential advantage can be diminished or even eliminated under suboptimal DSHP regulation. For example, the SP control logic (orange columns in Fig. 14) is advantageous only with very short BHE fields (50% of L_{nom}) but becomes much less effective as the borefield size increases. Conversely, with the ST and PCOP control logics, DSHPs can achieve a more significant improvement than traditional ASHPs and GCHPs. For example, with a single BHE 75 m long (50% undersizing), a DSHP adopting the ST or PCOP logics achieves up to 8% better annual performance than a GCHP coupled to the same borefield.

It might be expected that the PCOP logic, by consistently selecting the external source yielding the highest efficiency, would consistently outperform the ST logic. However, a closer analysis of the numerical

Table 10
Annual performance parameters in the tenth year of simulation for all the analyzed cases.

External source	Configuration	Heat absorbed from air/ground [kWh y^{-1}]	Building energy demand covered by air/ground [%]	Electric energy consumption [kWh y^{-1}]	$SCOP_{net}$	$SEER_{net}$	APF_{net}
Air (ASHP)	A	6578/−	100/−	7318	2.50	4.50	2.67
Ground (GCHP)	B1	−/8565	−/100	5488	3.33	6.81	3.60
	B2	−/8440	−/100	5614	3.25	6.77	3.52
	B3	−/8036	−/100	6025	3.02	6.61	3.28
	B4	−/7354	−/100	6709	2.70	6.20	2.94
Air + Ground (DSHP)	C1	2937/5693	19/81	5430	3.37	6.80	3.64
	C2	2934/5581	20/80	5537	3.30	6.75	3.56
	C3	4654/3611	31/69	5789	3.16	6.51	3.41
	C4	4647/3190	32/68	6218	2.94	6.06	3.17
	D1	3965/4236	27/73	5730	3.16	6.79	3.42
	D2	3951/4193	27/73	5789	3.12	6.73	3.39
	D3	3940/4004	27/73	6010	3.01	6.52	3.27
	D4	3963/3640	28/72	6388	2.84	6.10	3.08
	E1	684/7968	5/95	5410	3.39	6.80	3.65
	E2	888/7671	6/94	5505	3.32	6.76	3.59
	E3	1495/6770	10/90	5791	3.15	6.58	3.41
	E4	2218/5601	15/85	6240	2.92	6.14	3.16

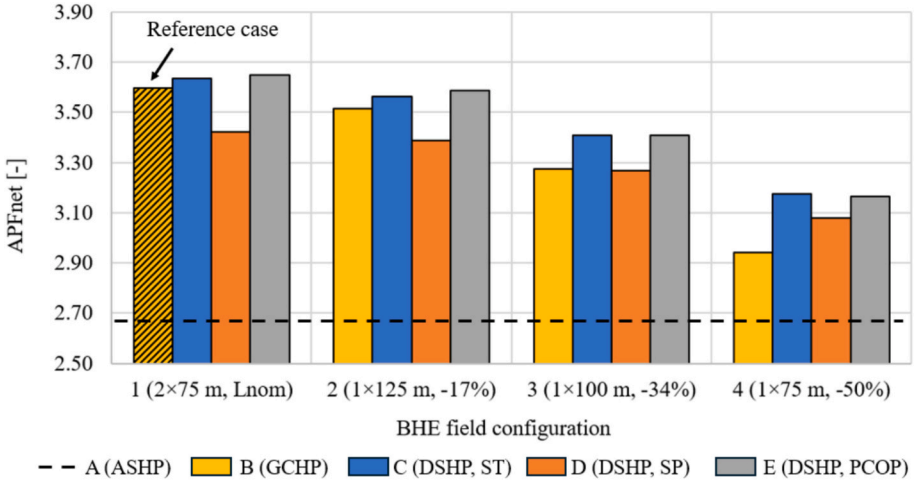

Fig. 14. Comparison of the APF_{net} values in the tenth year across the analyzed cases.

results shows a critical operating condition for the DSHP. An extract of the behavior of the DSHP coupled to a single 100 m long BHE and employing the PCOP logic over four hours during the tenth heating season is shown in Fig. 15.

In detail, Fig. 15 illustrates the DSHP activation profile (green curve) and the values of the outdoor air and geothermal fluid temperatures at the HP inlet (yellow and purple curves, respectively). Moreover, the instances when the DSHP triggers the operation into air-source and ground-source modes are indicated by yellow and purple circles, respectively. After the first start-up, the DSHP initially operates in geothermal mode for approximately 70 min, during which the BHE fluid temperature decreases until the *COP* in ground mode becomes lower than that in air mode, triggering a switch between the external sources. After 10 min of operation in air-source mode, the soil partially restores its thermal level, resulting again in the most efficient source and leading to another switch between the operating modes. However, due to the short recovery period exploited (only 10 min), the geothermal fluid temperature drops rapidly during the new operation in ground-source mode with such an undersized borefield. Since a minimum operating time of 10 min was selected for each source, during this period, the DSHP operates in geothermal mode with reduced efficiency. This behavior results in annual performance achieved through the PCOP logic just barely better than that obtained with the ST logic. As a consequence, to mitigate this inefficient operation, a potential

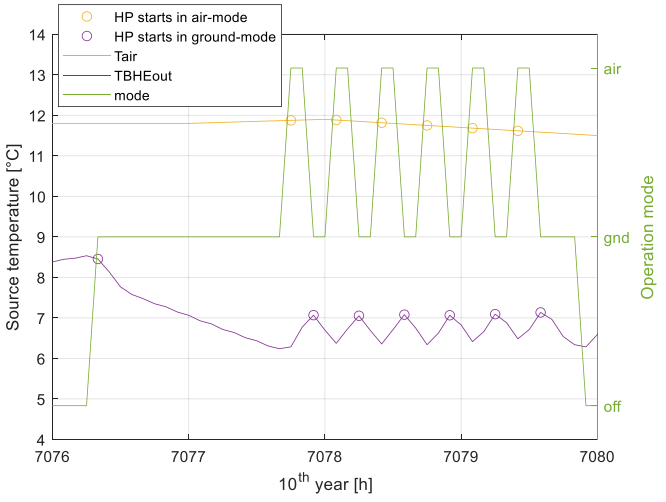

Fig. 15. Extract of the behavior of Case E3 during four hours of the tenth heating season.

improvement to the control logic would be to impose a minimum resting period for the soil of more than 10 min when the DSHP switches to air-source mode. During this recovery phase, the external air would serve as the heat source, even under less efficient conditions. However, it is noteworthy that the ambient air temperature remains more stable than the geothermal fluid temperature for a few-hour period (because the borefield is undersized), and, consequently, the *COP* in air mode is less subject to large fluctuations, allowing steady operations.

In conclusion, the greater implementation complexity of the PCOP logic does not appear to be justified when considering the energy performance achieved by the system with respect to that obtained with the ST logic (compare the APF_{net} values of the blue and grey bars in Fig. 14). However, a more detailed numerical model of the defrost process and the implementation of a larger minimum resting period for the ground could enhance the outcomes of the PCOP logic, making it a more attractive option. In this regard, the optimization of the PCOP logic will be analyzed in future research. On the other hand, the simplest SP control logic, although less efficient, may still be considered in the presence of a very short borefield (−50% nominal length), whilst it is not suitable for systems with larger borefield sizes.

5. Conclusions

In this study, the energy performance of a Dual-Source Heat Pump (DSHP), which can exploit aerothermal and geothermal energy alternately, was compared with those of a conventional Air-Source Heat Pump (ASHP) and a Ground-Coupled Heat Pump (GCHP) through long-term numerical simulations in the Matlab-Simulink environment. A building characterized by strongly unbalanced seasonal loads was selected, and simulations were carried out by using the open-source Simulink toolboxes ALMABuild and Carnot. Well-designed and significantly undersized (by up to 50%) Borehole Heat Exchanger (BHE) fields were coupled to the GCHP and DSHP to assess the influence of borefield size on the system efficiency. Moreover, since the selection of the optimal heat source is a crucial point for maximizing the performance of a DSHP, three control strategies were analyzed: (i) exploitation of the ambient air as external source when its temperature overcomes a threshold value called Switching Temperature (ST logic); (ii) use of the air/ground source during diurnal/nocturnal hours, respectively (SP logic); (iii) selection of the source based on the highest instantaneous *COP* (PCOP logic).

The main findings obtained are as follows:

- The ASHP exhibits the lowest performance (APF_{net} of 2.67), whereas the GCHP and DSHP yield 10–37% performance improvement;

- The source control logic and the borefield size play a significant role in the DSHP annual performance. The SP logic is slightly advantageous only with very undersized BHE fields, but becomes worse with increased borefield sizes;
- The higher the BHE field undersizing, the higher the advantage of using a DSHP with ST or PCOP control logic (with 50% undersizing, +8% in APF_{net} for the DSHP than the GCHP);
- The PCOP logic shows slightly better performance compared to the ST one, so its greater complexity in terms of hardware (i.e., temperature sensors) and software (i.e., computational requirements for the heat pump controller) does not appear justified.

The use of a DSHP proves to be competitive:

- To reduce the investment costs of the HVAC system by reducing the BHE field size with respect to the nominal length;
- To avoid the soil temperature drift with highly unbalanced building loads and/or undersized borefields (e.g., if the building undergoes a large volume expansion or change in the intended use, with consequent significant increase in the required loads), by replacing the heat generator only;
- To exploit the geothermal source even in the presence of limited drilling space.

The main limitations of the present work lie in the limited building thermal energy demand, the absence of Domestic Hot Water (DHW) production loads, and the need for further optimization of the PCOP logic. However, this article clearly demonstrates the potential energy savings achievable with DSHPs and the strong influence of the external source selection logic, paving the way for further studies. In this regard, future work is planned focusing on applications with higher energy demands (including DHW), such as those in the industrial and tertiary sectors, where the soil thermal deterioration can be even more significant, and DSHP control logics accounting for a more detailed defrosting model and a minimum ground resting period before a source switch higher than 10 min.

Declaration of competing interest

The authors declare that they have no known competing financial interests or personal relationships that could have appeared to influence the work reported in this paper.

Acknowledgements

This research was funded by R.d.S. - PTR 2025–2027 - LA 4.4 “Ottimizzazione di reti di teleriscaldamento urbano e distretti a energia positiva basati su pompe di calore di varia tipologia” - Progetto 1.7 - CUP Master I53C24003350001, CUP Locale J53C25003300005, and by the National Recovery and Resilience Plan (NRRP), Mission 4 Component 2 Investment 1.5—Call for tender No. 3277 of 30/12/2021 of Italian Ministry of University and Research funded by the European Union—NextGenerationEU; project code ECS00000033, Concession Decree No. 1052 of 23/06/2022 adopted by the Italian Ministry of University and Research, CUP D93C22000460001, “Ecosystem for Sustainable Transition in Emilia- Romagna” (Ecosister), Spoke 4.

Data availability

Data will be made available on request.

References

[1] M. Tao, Z. Gou, N. Ma, Assessment of thermal comfort and thermal resilience in dwellings during heat waves: a case study of a near-zero energy house, J. Build. Eng. 109 (2025) 113052, https://doi.org/10.1016/j.jobe.2025.113052.
[2] V.V. Yurak, S.A. Fedorov, Review of natural and anthropogenic emissions of carbon dioxide into the earth's atmosphere, Int. J. Environ. Sci. Technol. 22 (2025) 2719–2736, https://doi.org/10.2139/ssrn.5038332.
[3] M. Gourovitch, B. Laratte, J.P. Costes, A strong straw policy can supply three quarters of the insulation needs for construction and renovation in France, Energ. Buildings 344 (2025) 116013, https://doi.org/10.1016/j.enbuild.2025.116013.
[4] M. Yousefi, M. Pahn, Case study on multifunctional building parts: integration, simulation, and performance analysis in sustainable residential environments, J. Build. Eng. 100 (2025) 111807, https://doi.org/10.1016/j.jobe.2025.111807.
[5] E. Schito, P. Conti, Energy savings potential of multipurpose heat pumps in air-handling systems, Energies 18 (2025) 3259, https://doi.org/10.3390/en18133259.
[6] E. Osterman, U. Stritih, Review on compression heat pump systems with thermal energy storage for heating and cooling of buildings, J. Energy Storage 39 (2021) 102569, https://doi.org/10.1016/j.est.2021.102569.
[7] D. Bogdanov, R. Satymov, C. Breyer, Impact of temperature dependent coefficient of performance of heat pumps on heating systems in national and regional energy systems modelling, Appl. Energy 371 (2024) 123647, https://doi.org/10.1016/j.apenergy.2024.123647.
[8] N. Aste, P. Caputo, C. Del Pero, G. Ferla, H.E. Huerto-Cardenas, F. Leonforte, A. Miglioli, A renewable energy scenario for a new low carbon settlement in northern Italy: biomass district heating coupled with heat pump and solar photovoltaic system, Energy 206 (2020) 118091, https://doi.org/10.1016/j.energy.2020.118091.
[9] EurObservER, Heat pumps barometer 2024, Accessed on 04/12/2025, available online: https://www.eurobserv-er.org/heat-pumps-barometer-2024/, 2024.
[10] Y. Xu, R. Zhao, K. Wu, H. Jin, M. Song, X. Shen, Experimental investigation and validation on an air-source heat pump frosting state recognition method based on fan current fluctuation signal and machine learning, Energy 291 (2024) 13037, https://doi.org/10.1016/j.energy.2024.130372.
[11] A.A. Serageldin, Y. Sakata, T. Katsura, K. Nagano, Performance enhancement of borehole ground source heat pump using single u-tube heat exchanger with a novel oval cross-section (SUO) and a novel spacer, Sustain. Energy Techn. and Assess. 42 (2020) 100805, https://doi.org/10.1016/j.seta.2020.100805.
[12] E. Bisengimana, J. Zhou, M. Binama, K. Zhao, S. Abbas, Y. Yuan, The frosting and soil imbalance performance issues of building heat pumps: an overview, Energ. Buildings 273 (2022) 112387, https://doi.org/10.1016/j.enbuild.2022.112387.
[13] Y. Shimada, K. Tokimatsu, T. Asawa, Y. Uchida, A. Tomigashi, H. Kurishima, Subsurface utilization as a heat sink for large-scale ground source heat pump: case study in Bangkok, Thailand, Renew. Energy 180 (2021) 966–979, https://doi.org/10.1016/j.renene.2021.08.116.
[14] R. Lazzarin, Heat pumps and solar energy: a review with some insights in the future, Int. J. Refrig. 116 (2020) 146–160, https://doi.org/10.1016/j.ijrefrig.2020.03.031.
[15] S. Marinelli, F. Lolli, M.A. Butturi, B. Rimini, R. Gamberini, Environmental performance analysis of a dual-source heat pump system, Energ. Buildings 223 (2020) 110180, https://doi.org/10.1016/j.enbuild.2020.110180.
[16] J. Marchante-Avellaneda, E. Navarro-Peris, Y. Song, Development of map-based models for the performance characterization in a new prototype of dual source heat pump, Appl. Therm. Eng. 236 (Part C) (2024) 121743, https://doi.org/10.1016/j.applthermaleng.2023.121743.
[17] J.M. Corberan, A. Cazorla-Marin, J. Marchante-Avellaneda, C. Montagud, Dual source heat pump, a high efficiency and cost-effective alternative for heating, cooling and DHW production, Int. J. Low-Carbon Technol. 13 (2018) 161–176, https://doi.org/10.1093/ijlct/cty008.
[18] J. Cao, L. Zheng, J. Peng, W. Wang, M.K.H. Leung, Z. Zheng, M. Hu, Q. Wang, J. Cai, G. Pei, J. Ji, Advances in coupled use of renewable energy sources for performance enhancement of vapour compression heat pump: a systematic review of applications to buildings, Appl. Energy 332 (2023) 120571, https://doi.org/10.1016/j.apenergy.2022.120571.
[19] M. Bottarelli, M. Bortoloni, Y. Su, On the sizing of a novel flat-panel ground heat exchanger in coupling with a dual-source heat pump, Renew. Energy 142 (2019) 552–560, https://doi.org/10.1016/j.renene.2019.04.088.
[20] X. Guo, H. Wei, X. He, J. Du, D. Yang, Experimental evaluation of an earth–to–air heat exchanger and air source heat pump hybrid indoor air conditioning system, Energ. Buildings 256 (2022) 111752, https://doi.org/10.1016/j.enbuild.2021.111752.
[21] B. Panigrahi, C.W. Chang, W.C. Hsieh, W.J. Luo, Heating and defrosting performance assessment of dual-source heat pump operational modes under various ambient conditions, J. Build. Eng. 89 (2024) 109359, https://doi.org/10.1016/j.jobe.2024.109359.
[22] P. Adebayo, C. Beragama Jathunge, A. Darbandi, N. Fry, R. Shor, A. Mohamad, C. Wemhöner, A. Mwesigye, Development, modeling, and optimization of ground source heat pump systems for cold climates: a comprehensive review, Energ. Buildings (2024) 114646, https://doi.org/10.1016/j.enbuild.2024.114646.
[23] Q. Yu, Z. Yang, J. Song, F. Xing, J. Zhou, H. Qi, Modeling and operational characteristics analysis of a dual-source synergetic heat pump based on air energy and biomass waste heat, Energy 309 (2024) 133087, https://doi.org/10.1016/j.energy.2024.133087.
[24] T. Reum, D. Schmitt, T. Summ, C. Trinkl, F. Ochs, T. Schrag, Experimental analysis of parallel operation of two heat sources in a dual-source heat pump incorporating two compressors, Int. J. Refrig. 171 (2025) 124–138, https://doi.org/10.1016/j.ijrefrig.2024.12.013.
[25] R. Lazzarin, M. Noro, Photovoltaic/thermal (PV/T)/ground dual source heat pump: optimum energy and economic sizing based on performance analysis, Energ. Buildings (2020) 109800, https://doi.org/10.1016/j.enbuild.2020.109800.

[26] J.L. Wang, T. Yan, X. Tang, W.G. Pan, Design and operation of hybrid ground source heat pump systems: a review, Energy 316 (2025) 13453, https://doi.org/10.1016/j.energy.2025.134537.
[27] A. Zarrella, R. Zecchin, P. Pasquier, D. Guzzon, E. Prataviera, L. Vivian, M. De Carli, G. Emmi, Analysis of retrofit solutions of a ground source heat pump system: an italian case study, Energies 13 (21) (2020) 5680, https://doi.org/10.3390/en13215680.
[28] L. Zhang, G. Feng, A. Li, K. Huang, S. Chang, Comprehensive evaluation and analysis of a nearly zero-energy building heating system using a multi-source heat pump in severe cold region, Build. Simul. 16 (2023) 1949–1970, https://doi.org/10.1007/s12273-023-0990-8.
[29] I. Grossi, M. Dongellini, A. Piazzi, G.L. Morini, Dynamic modelling and energy performance analysis of an innovative dual-source heat pump system, Appl. Therm. Eng. 142 (2018) 745–759, https://doi.org/10.1016/j.applthermaleng.2018.07.022.
[30] S. Bordignon, M. Marigo, M. De Carli, A. Zarrella, Evaluation of control strategies for a dual-source heat pump, Sci. Technol. Built Environ. (2025) 1–12, https://doi.org/10.1080/23744731.2025.2530357.
[31] E. Zanetti, S. Bonduà, S. Bortolin, V. Bortolotti, M. Azzolin, F. Tinti, Sequential coupled numerical simulations of an air/ground-source heat pump: validation of the model and results of yearly simulations, Energ. Buildings 277 (2022) 112540, https://doi.org/10.1016/j.enbuild.2022.112540.
[32] A. Jahanbin, U. Berardi, A hybrid machine learning framework for optimizing heat pump-driven domestic hot water systems based on user behaviour and control strategies, Appl. Therm. Eng. 279 (2025) 127664, https://doi.org/10.1016/j.applthermaleng.2025.127664.
[33] H. Liu, Z. Fang, S. Yang, C. Mao, Z. Wang, Z. Chen, S. Yang, P. Duan, Application analysis of hybrid heat pump heating systems optimized with deep reinforcement learning control, J. Build. Eng. 113 (2025) 114024, https://doi.org/10.1016/j.jobe.2025.114024.
[34] W. Zhang, Y. Yu, Z. Yuan, P. Tang, B. Gao, Data-driven pre-training framework for reinforcement learning of air-source heat pump (ASHP) systems based on historical data in office buildings: field validation, Energ. Buildings 332 (2025) 115436, https://doi.org/10.1016/j.enbuild.2025.115436.
[35] C. Natale, M. Dongellini, C. Naldi, G.L. Morini, Evaluation of the seasonal energy performance of a dual-source heat pump through dynamic experimental tests, Energies 18 (2025) 2532, https://doi.org/10.3390/en18102532.
[36] R. Dott, M.Y. Haller, J. Ruschenburg, F. Ochs, J. Bony, The reference framework for system simulations of the IEA SHC task 44 / HPP annex 38 part b, Build. Space Heat Load (2013), https://doi.org/10.13140/2.1.2221.4727.
[37] D.P.R N. 412, Regulations Establishing Standards for the Design, Installation, Operation and Maintenance of Thermal Systems in Buildings for the Purpose of Containing Energy Consumption, Rome, Italy, 1993.
[38] J.P. Campana, G.L. Morini, BESTEST and EN ISO 52016 benchmarking of ALMABuild, a new open-source simulink tool for dynamic energy modelling of buildings, Energies 12 (2019) 2938, https://doi.org/10.3390/en12152938.
[39] J.P. Campana, ALMABEST: a new whole building energy simulation simulink-based tool for NZEB design, PhD dissertation, supervisor: Gian luca morini, Alma Mater Studiorum - University of Bologna (2019), https://doi.org/10.6092/unibo/amsdottorato/8993.
[40] Comitato Termotecnico Italiano, Test Reference Year, available online, https://try.cti2000.it/, 2025.
[41] M. Song, S. Deng, C. Dang, N. Mao, Z. Wang, Review on improvement for air source heat pump units during frosting and defrosting, Appl. Energy 211 (2018) 1150–1170, https://doi.org/10.1016/j.apenergy.2017.12.022.
[42] M. Soltani, P. Farzanehkhameneh, F.M. Kashkooli, A. Al-Haq, J. Nathwani, Optimization and energy assessment of geothermal heat exchangers for different circulating fluids, Energy Convers. Manag. 228 (2021) 113733, https://doi.org/10.1016/j.enconman.2020.113733.
[43] G. Krakat, VDI Heat Atlas, 2nd ed, Springer, Mülheim, Ruhr, 2010, p. 451.
[44] P.L.U.S. Termoplast, Pre-mixed for the filling of geothermal wells, Technical Datasheet, Accessed on 04/12/2025, available online, https://www.gtssnc.com/schedetecniche/premiscelato_Termoplast_PLUS.pdf, 2024.
[45] ASHRAE Handbook 2007 – HVAC applications 32, ASHRAE, Atlanta, GA, 2007.
[46] L. Lamarche, S. Kajl, B. Beauchamp, A review of methods to evaluate borehole thermal resistances in geothermal heat-pump systems, Geothermics 39 (2010) 187–200, https://doi.org/10.1016/j.geothermics.2010.03.003.
[47] CARNOT, Toolbox Ver. 7. 3, for Matlab/Simulink R2018b, © Solar-Institut Jülich, 2022.
[48] E. Zanchini, S. Lazzari, Temperature distribution in a field of long borehole heat exchangers (BHEs) subjected to a monthly averaged heat flux, Energy 59 (2013) 570–580, https://doi.org/10.1016/j.energy.2013.06.040.
[49] J. Claesson, S. Javed, An analytical method to calculate borehole fluid temperatures for time-scales from minutes to decades, ASHRAE Trans 117 (2011) 279–288.
[50] C. Naldi, E. Zanchini, Effects of the total borehole length and of the heat pump inverter on the performance of a ground-coupled heat pump system, Appl. Therm. Eng. 128 (2018) 306–319, https://doi.org/10.1016/j.applthermaleng.2017.09.025.
[51] P. Eskilson, Thermal Analysis of Heat Extraction Boreholes, PhD dissertation, University of Lund (S), 1987.
[52] P. Vocale, G.L. Morini, M. Spiga, Influence of outdoor air conditions on the air source heat pumps performance, Energy Procedia 45 (2014) 653–662, https://doi.org/10.1016/j.egypro.2014.01.070.
[53] Carnot User Manual, Accessed on 27/03/2025, available online, https://fh-aachen.sciebo.de/s/j8ZF9nP1nySPTfh, 2025.
[54] W. Wang, Y.C. Feng, J.H. Zhu, L.T. Li, Q.C. Guo, W.P. Lu, Performances of air source heat pump system for a kind of mal-defrost phenomenon appearing in moderate climate conditions, Appl. Energy 112 (2013) 1138–1145, https://doi.org/10.1016/j.apenergy.2012.12.054.
[55] M. Milanowski, A. Cazorla-Marín, C. Montagud-Montalvá, Energy analysis and cost-effective design solutions for a dual-source heat pump system in representative climates in europe, Energies 15 (22) (2022) 8460, https://doi.org/10.1016/j.enbuild.2022.112540.